

A CATALOG OF HOLES AND SHELLS IN THE INTERSTELLAR MEDIUM OF THE LITTLE THINGS DWARF GALAXIES

NAU RAJ POKHREL,^{1,2} CAROLINE E. SIMPSON,¹ AND IOANNIS BAGETAKOS³

¹*Department of Physics, Florida International University, 11200 SW 8th St., Miami, FL 33199, USA*

²*Department of Physics and Astronomy, The University of Tennessee, 1408 Circle Drive, Knoxville, TN 37996, USA*

³*ASTRON, the Netherlands Institute for Radio Astronomy, Postbus 2, 7990 AA, Dwingeloo, The Netherlands*

ABSTRACT

We present a catalog of holes and shells in the neutral atomic hydrogen (H I) of 41 gas-rich dwarf galaxies in LITTLE THINGS (Local Irregulars That Trace Luminosity Extremes, The H I Nearby Galaxy Survey). We analyzed their properties as part of an investigation into the relation between star formation and structures and kinematics in the H I of small galaxies. We confirmed 306 holes between 38 pc (our resolution limit) and 2.3 kpc, with expansion velocities up to 30 km s⁻¹. The global star formation rates measured by H α and FUV emission are consistent with those estimated from the energy required to create the cataloged holes in our sample. Although we found no obvious correlation between global star-formation rates and the H I surface and volume porosities of our sample, two of the four lowest porosity galaxies and the two highest porosity galaxies have no recent star formation as measured by H α and FUV emission.

arXiv:2006.01735v1 [astro-ph.GA] 2 Jun 2020

1. INTRODUCTION

Dwarf galaxies are the most abundant and dynamically the simplest galaxy systems in the Universe, having a wide range of morphology and physical properties. Dwarfs are also low mass, ranging in mass from 10^6 to $10^{10} M_\odot$, with shallower gravitational potentials and thicker disks than spirals (Mateo 1998; Tolstoy et al. 2009; Hunter et al. 2012; Klein 2012). They are small in size (1 to 10 kpc in diameter) and have low luminosities ranging from $-5 \gtrsim M_B \gtrsim -18$ (Mateo 1998; Tolstoy et al. 2009; Simon 2019). These galaxies rotate with low rotational speed (10 to 100 km s $^{-1}$) and generally possess solid body rotation (Mateo 1998; Tolstoy et al. 2009; Hunter et al. 2012; Klein 2012).

Dwarf galaxies are believed to be the earliest-forming galaxies and the building blocks for larger systems (Kauffmann et al. 1993, 1996). By studying dwarf galaxies, we can get a better picture of the evolution of galaxies (Tolstoy et al. 2009).

Among dwarfs, we are interested in dwarf irregulars because of their primitive structure, and their role in galaxy formation. Although dwarf irregular galaxies have little dust and low metallicity even in their central regions, they are rich in neutral atomic hydrogen gas in comparison to spirals (Karachentsev et al. 2004), and hence are the ideal laboratories to study the star-gas interaction in star formation, the evolution of galaxies, and hence the evolution of the early universe (Cowie et al. 1996; Skillman 1996; Dohm-Palmer et al. 1997; Mateo 1998; van den Bergh 2000; Karachentsev et al. 2004; Thomas et al. 2005; Weisz et al. 2009b).

The critical gas density of any galaxy is the column density of galactic disk gas above which the disk becomes unstable and can collapse to form stars (Kennicutt 1989). In irregular galaxies, the ratio of the observed gas density to the critical gas density is two to three times lower than that of spirals in the inner region as well as beyond the outer radius where star formation apparently ends (Hunter & Plummer 1996; Hunter et al. 1998). Studies of the ionized hydrogen gas (H II) in dwarfs shows that dwarf galaxies have star-forming regions as large as those in spirals and they are forming stars not only in the densest inner region, but also in the far outer parts (Hunter 1982; Hunter et al. 1998). It is important to understand how the H I gas collapses and forms stars in such simple systems to understand the evolution of galaxies.

1.1. History of H I Structure Studies

Neutral hydrogen structures were first found by Westerlund & Mathewson (1966) in the ISM of the Large Magellanic Cloud, followed by Hindman (1967) in the Small Magellanic Cloud, who suggested that the cause of such structures might be ‘super supernovae.’ Following the survey by Weaver & Williams (1973), Heiles (1976) discovered expanding H I holes in the Milky Way as expected in the theoretical explanation by Cox & Smith (1974), and McKee & Ostriker (1977). Later, Heiles (1979, 1984) and Hu (1981) prepared catalogs of expanding H I holes in the Milky Way. Studies by Brinks & Bajaja (1986), Puche et al. (1992), Kim et al. (1999), Walter & Brinks (1999), Chu et al. (2008), Warren et al. (2011) and many others detected or/and analyzed the possible origins and properties of H I shells, holes, or bubble-like structures. Some galaxies have an ISM that is dominated by such structures, which might have been formed by a single or a combination of various processes such as stellar feedback, i.e., stellar winds and supernovae (SNe) explosions (Weaver et al. 1977; Cash et al. 1980; McCray & Kafatos 1987; Tenorio-Tagle et al. 1988; Ott et al. 2001; Simpson et al. 2005a; Weisz et al. 2009a,b; Cannon et al. 2011), from turbulence in the ISM, i.e., the motion of high velocity gas (Tenorio-Tagle 1981; Tenorio-Tagle et al. 1988; Rand & Stone 1996; Santillán et al. 1999; Murray & Lin 2004), a high-energy gamma-ray burst (Efremov et al. 1998; Loeb & Perna 1998; Perna & Raymond 2000), or thermal and gravitational instabilities (Dib & Burkert 2005).

Relaño et al. (2007) proposed that H I holes are originated from H II regions. The explanation of multiple supernovae explosions was supported by Weisz et al. (2009b) while studying the H I holes in Holmberg II. The estimated age and the mechanical luminosity of the possible clusters which might have created the holes suggests that the combined effect of multiple supernovae might be the cause of H I hole formation (Chakraborti & Ray 2011). The correlation between the H I holes and the stars is in agreement with Chakraborti & Ray (2011); Ehlerová & Palouš (2013); Suad et al. (2014). Ehlerová & Palouš (2016) suggest that the estimated amount of energy required to create the large holes should be from the multiple supernovae of OB associations. The study of the large H I shells in the outer part of Milky Way indicates that the stellar wind combined with another energy source might be responsible to create such structures (Suad et al. 2014, 2016).

The numerical simulation of Dib & Burkert (2005) suggests that the H I holes in dwarf irregulars can form as a combined result of turbulence, thermal instabilities, and gravitational instabilities whereas the simulation of Vorobyov & Basu (2005) shows that stellar feedback (multiple SNe or a hypernova explosion associated with gamma ray burst,

and the vertical impact of an high velocity cloud) describes the formation of H I holes with more accuracy than the other processes (Warren et al. 2011). The result of Park et al. (2016) shows that the impact of high-velocity clouds (HVCs) falling into the galactic disk or OB association could be the factor to create H I structures.

1.2. The Role of Stellar Feedback in H I Structure Formation

The energy estimate required to form H I holes ranges from 10^{50} to 10^{54} erg, which is derived from the measured expansion velocities (v_{exp}). Although observations show that holes are smaller than predicted by the estimation of adiabatic evolution, stellar feedback is still considered to play an important role in H I structure formation because this theory is based on shock-heated ($\geq 10^6$ K) pressure. It has some uncertainty such as growth rate discrepancy which may be due to the inhomogeneity of the ISM, energy transfer from the holes to cosmic rays, overestimation of input energy, and/or underestimation of ambient density/pressure (Castor et al. 1975; Dyson 1977; Oey 2007).

The comparison of 21 cm H I observations with those at other wavelengths provides a better understanding of hole formation, gas dynamics, and the relation between structures in the H I and stellar feedback. Some works of the comparison of H I and H α images are in Kennicutt et al. (1995), Martin (1998), Walter et al. (2002), Pidopryhora et al. (2007); and wavelet analyses are in Frick et al. (2001), Hughes et al. (2006), Tabatabaei et al. (2007) and Dumas et al. (2011). Currently, infrared images (older stellar populations) from the Spitzer Space Telescope and ultraviolet images (younger star-forming regions) from the Galaxy Evolution Explorer (*GALEX*) satellite telescope are the most widely used to compare with H I maps.

In the comparison of images at different wavelengths, we expect that the smaller and the younger holes might also have H α emission from active star formation regions, whereas the shells of the older and the larger holes might be filled with O and B stars emitting UV radiation. For more metal-rich galaxies (such as spirals), we also expect CO emission from the outer rims of the expanding holes where molecular clouds are being compressed (Deharveng et al. 2009; Bagetakos et al. 2011).

The exact cause of the formation of H I holes is still not clear. Our study starts with cataloging such structures in our sample galaxies to study their properties and relate them to star formation feedback. In this project, we study the kinematics of H I holes/shells in a sample of nearby dwarf galaxies, investigate the effect of global porosity in the H I on star formation rates, and examine whether the observed H I structures are likely to be related to star-formation activity.

2. DATA: GALAXY SAMPLE AND OBSERVATIONS

For this study, we use data from the LITTLE THINGS¹ (Local Irregulars That Trace Luminosity Extremes, The H I Nearby Galaxy Survey) project, which looks at star formation processes in dwarf galaxies. The LITTLE THINGS sample contains 41 gas-rich, non-interacting, relatively isolated nearby dwarf galaxies with a wide range of properties. Among them, 37 are dwarf irregulars (dIrrs) and the rest are blue compact dwarfs (BCDs), as listed in Table 1. The average distance of LITTLE THINGS galaxies is 3.7 Mpc, with the nearest and the farthest galaxies, NGC 6822 and DDO 52, at distances of 0.5 Mpc and 10.3 Mpc respectively. The LITTLE THINGS multiband data set includes H I observations obtained with the National Radio Astronomy Observatory (NRAO) NSF's Karl G. Jansky Very Large Array (VLA)². These data have high sensitivity (≤ 1.1 mJy beam⁻¹ channel⁻¹), high angular resolution ($\approx 6''$), and high velocity resolution. The H I data for 20 galaxies are taken from the VLA archives, with 2.6 km s⁻¹ channel separation; the separation is 1.3 km s⁻¹ for the new data obtained from the VLA in the B, C and D array configurations by the LITTLE THINGS group. The angular resolution limit of $6''$ corresponds to linear resolutions ranging from ≈ 26 to 300 pc with 110 pc at the average distance at 3.7 Mpc.

AIPS (Astronomical Image Processing System) was used to calibrate and map the observed data. More detail about the observation and calibration of the H I data is described in Hunter et al. (2012). Both natural-weighted (NA) and robust-weighted (RO) H I data cubes were made using the task IMAGR in AIPS. By adjusting the beam size during mapping, i.e., adjusting the weighting of data from different baseline lengths, H I data can be mapped at different sensitivities and resolutions. Natural weighting is used to produce images with lower noise/higher sensitivity. However, such images have lower resolution because the (more numerous) data from shorter baselines (lower resolution) are more heavily weighted than the (scattered) data from longer baselines. Robust weighting allows the user to adjust

¹ <https://science.nrao.edu/science/surveys/littlethings>

² NRAO is a facility of the National Science Foundation operated under cooperative agreement by Associated Universities, Inc. These data were taken during the upgrade of the VLA to the Expanded VLA or EVLA, now named the Karl G. Jansky Very Large Array.

the weighting of data from different baseline lengths. By more heavily weighting data from longer baselines, images with higher resolution but lower sensitivity (due to increased noise) are produced.

For this project, the natural-weighted flux density maps and data cubes are initially used to find the structures (holes, shells etc.) in the sample and to study low density gas around those structures. If they are not detailed enough, robust-weighted maps and data cubes are helpful in such cases, as discussed below.

In addition to the H I data, we also use data of other wavelengths to get information about the population of stars of different ages. **The FUV data are from *GALEX*, and H α data are from Hunter & Elmegreen (2004, 2006).**

3. H I STRUCTURE (“HOLE”) DETECTION METHOD

Both automated detection algorithms and visual inspection methods are used to detect H I holes in galaxies. Thilker et al. (1998) used expanding models to detect holes in NCG 2403 whereas Mashchenko et al. (2002) used 3D hydrodynamical simulations to discover holes in the same galaxy. Daigle et al. (2003) used a neural network algorithm based on velocity spectra to identify such structures. Later on, Ehlerová & Palouš (2005, 2013) discovered holes in the Milky Way by using a hole-searching algorithm on data from Leiden-Dwingeloo and Leiden-Argentine-Bonn surveys. Sallmen et al. (2015) visually inspected the SETHI database to detect H I holes in the Milky Way and cataloged 74 previously unidentified H I structures. The catalog includes the physical properties such as the locations, radial velocities, physical sizes, and estimated the energy required to form those structures.

The automated algorithms are efficient when the parameters are identical and the structures are regular, symmetric and complete. However, such structures in galaxies have various shapes, and the data sensitivity and resolution for each sample also varies. This variation would require individual automated models for each galaxy, but this would reduce the consistency of the method. Therefore, the visual observation method gives a more consistent outcome for the discovery of holes in spite of its certain subjective biases (Bagetakos et al. 2011).

We agree with Bagetakos et al. (2011) that automated methods don’t provide a satisfactory outcome when searching for such irregular structures. Therefore, we preferred visual observation over automated algorithms and searched for holes in the LITTLE THINGS sample as in Bagetakos et al. (2011). The H I structure in five galaxies of our sample (**DDO 50, DDO 53, DDO 63, DDO 154, and NGC 4214**) were studied by Bagetakos et al. (2011). These galaxies were examined for structures independently at first to make a ‘standard’ visual inspection technique. This technique was then used on the entire galaxy sample to create a catalog of H I structures (holes and shells). We used the KARMA³ visualization software package to identify the H I holes in the galaxies **and recorded 1181 possible holes as the first identification**. We extensively used tasks KVIS and KPVSLICE to display our data, to characterize the holes in each region of the galaxies, and to analyze their various properties.

3.1. Observed Properties

In the first step, with KVIS, we searched for holes visually in the natural-weighted integrated H I maps of the entire galaxy sample and delineated them with ellipses. The coordinates of the center of the hole (in right ascension and declination, J2000) are taken as the pixel having the minimum flux density inside the ellipse closest to the visual center. For consistency, we used the same color and intensity scale throughout the sample. To approximate the flux density of those regions before the holes were created, we selected an area approximately twice the area of the hole and averaged the total flux. The estimated uncertainty of the flux is from the uncertainty of the center of the hole which is of order 10%. For the quality measure of the holes, the most distinct holes with a distinct density gradient are given 3 points, down to 0 points for the most indistinct holes.

In the second step, we used the robust-weighted integrated H I maps and repeated the same process as in the first. Because of the high resolution of the data, much more structure is visible but not every structure is a hole, which makes proper identification of holes more difficult, so the highest quality measure is assigned as 2. We did detect some holes in the robust-weighted maps which were not seen in the natural-weighted maps due to the lower resolution (as an example, holes in F564-V3). Half of the beam size (of order 3”) is taken as the uncertainty of the position center of the holes in each case.

³ <http://www.atnf.csiro.au/computing/software/karma/>

Table 1. Basic Galaxy Information

Galaxy	RA (J2000)	Dec (J2000)	Distance ^a	PA ^a	Inclination ^a	R_D ^b
	(hh mm ss.s)	(dd mm ss)	(Mpc)	(deg)	(deg)	(kpc)
CVnIdwA	12 38 40.2	+32 45 40	3.6	80	41.0	0.57
DDO 43	07 28 17.8	+40 46 13	7.8	6.5	48.5	0.41
DDO 46	07 41 26.6	+40 06 39	6.1	84	28.6	1.14
DDO 47	07 41 55.3	+16 48 08	5.2	−70	64.4	1.36
DDO 50	08 19 08.7	+70 43 25	3.4	18	46.7	1.10
DDO 52	08 28 28.5	+41 51 21	10.3	5	51.1	1.32
DDO 53	08 34 08.0	+66 10 37	3.6	81	64.4	0.72
DDO 63	09 40 30.4	+71 11 02	3.9	0	0	0.68
DDO 69	09 59 25.0	+30 44 42	0.8	−64	60.3	0.19
DDO 70	10 00 00.9	+05 19 50	1.3	88	57.8	0.48
DDO 75	10 10 59.2	−04 41 56	1.3	41	33.5	0.22
DDO 87	10 49 34.7	+65 31 46	7.7	76.5	58.6	1.31
DDO 101	11 55 39.4	+31 31 08	6.4	−69	49.4	0.93
DDO 126	12 27 06.5	+37 08 23	4.9	−41	67.7	0.87
DDO 133	12 32 55.4	+31 32 14	3.5	−6	49.4	1.24
DDO 154	12 54 06.2	+27 09 02	3.7	46	65.2	0.59
DDO 155	12 58 39.8	+14 13 10	2.2	51	47.6	0.15
DDO 165	13 06 25.3	+67 42 25	4.6	89	61.9	2.26
DDO 167	13 13 22.9	+46 19 11	4.2	−23	52.8	0.33
DDO 168	13 14 27.2	+45 55 46	4.3	−24.5	54.5	0.83
DDO 187	14 15 56.7	+23 03 19	2.2	37	39.0	0.18
DDO 210	20 46 52.0	−12 50 50	0.9	−85	66.9	0.17
DDO 216	23 28 35.0	+14 44 30	1.1	−58	69.4	0.54
F564-V3	09 02 53.9	+20 04 29	8.7	7	35.8	0.53
Haro 29	12 26 16.7	+48 29 38	5.8	85	58.6	0.29
Haro 36	12 46 56.3	+51 36 48	9.3	2	37.9	0.68
IC 10	00 20 21.9	+59 17 39	0.7	−38	41.0	0.40
IC 1613	01 04 49.2	+02 07 48	0.7	71	37.9	0.58
LGS 3	01 03 55.2	+21 52 39	0.7	−3.5	64.4	0.23
M81dwA	08 23 57.2	+71 01 51	3.5	86	45.8	0.25
Mrk 178	11 33 29.0	+49 14 24	3.9	−50	68.6	0.33
NGC 1569	04 30 49.8	+64 50 51	3.4	−59	61.1	0.39
NGC 2366	07 28 48.8	+69 12 22	3.4	32.5	72.1	1.35
NGC 3738	11 35 49.0	+54 31 23	4.9	0	0	0.78
NGC 4163	12 12 09.2	+36 10 13	2.9	18	53.7	0.27
NGC 4214	12 15 39.2	+36 19 38	3.0	16	25.8	0.75
NGC 6822	19 44 57.9	−14 48 11	0.5	24	...	0.57
SagDIG	19 30 00.6	−17 40 56	1.1	87.5	62.7	0.23
UGC 8508	13 30 44.9	+54 54 29	2.6	−60	61.9	0.26
WLM	00 01 59.2	−15 27 41	1.0	−2	70.3	0.57
VIIZw 403	11 27 58.2	+78 59 39	4.4	−10	66.0	0.52

^a Hunter et al. (2012)^b V-band scale length from Hunter & Elmegreen (2004)

In the third step, we viewed each velocity channel map on rapid slide show (a ‘movie’) of the natural-weighted cube files and overlaid the ellipses drawn from the first and second steps. Only holes present in three or more consecutive channels were considered genuine. The centers of the holes were further examined with the help of channel maps to confirm that these are actual holes and not just low density regions. Another reason to view each channel map was to search for possibly ‘hidden’ intact holes. These fully-contained holes can be detected well in the position-velocity diagrams and the channel maps. We quantified the quality of holes in this part as: Holes found in zero to two consecutive channels got no points. Holes seen in three to four consecutive channels got 1 point. If they are in five to seven consecutive channels they were given 2 points, and for more than seven channels we classified them as distinct holes with 3 points.

In the final step, we worked with task KPVSLICE to further quantify and analyze interactive position-velocity (pv) slices and intensity profiles through each hole in the data cubes of the sample galaxies. Intensity profiles are the flux density distribution along a slice through the center of a hole. An example of a hole in NGC 4214 is shown in Figure 1. Since the slices are freely definable in KPVSLICE and the line of cut can be rotated by any angle at the center of the ellipse drawn around the holes, we can identify the major/minor axes of the ellipse and measure them to determine the full-width half-maximum (FWHM) of the intensity profile. The measurements are verified simultaneously in both the pv diagrams and the intensity profiles. The uncertainty on the axes is of order $3''$ which is estimated as the half of the robust beam size. We also measured the position angle (PA) of the major axis from north through east. We estimated an uncertainty of order 20° with multiple independent measurements. The ratio of the minor-to-major axis is the axial ratio of the hole with uncertainty of order 25% on the basis of repeated independent measurements.

The heliocentric (systemic) velocity (v_{Hel}) of the hole was taken as the velocity channel where the contrast between the hole and its edge is highest (i.e., where the clearest feature is seen) in the pv diagram. The velocity resolution (1.3 or 2.6 km s^{-1}) is taken as an error estimation.

All the holes are classified into three groups as in Figure 2 using the interactive pv diagram and intensity profile following Brinks & Bajaja (1986), and Bagetakos et al. (2011). Type 1 holes are completely ‘blown out’ holes where there is no gas visible on either the low or the high velocity side of the hole (Figure 1). Type 2 holes are partially blown out. They have visible gas deviating from the surrounding gas towards higher or lower velocities on one side, whereas the other side is characterized by lack of gas as shown in the pv diagram. Type 3 holes are intact, where both sides can be seen in the pv diagram. It is expected that the expansion of Type 3 holes leads to the formation of Type 2 holes. Because Type 1 holes are generally larger than Type 2 and Type 3 (Bagetakos et al. 2011), they are thought to be blown out and therefore are farther along the evolution process.

The expansion velocity (v_{exp}) of a hole is found by measuring the deviation of the velocity of the gas as seen in a pv diagram. The expansion velocity can’t be measured for completely broken (Type 1) holes. An upper limit of v_{exp} for these holes was estimated from the average velocity dispersion of a nearby, quiescent region of the second moment map of the galaxy. For Type 2 holes, we calculated v_{exp} as the difference between the v_{Hel} and the gas velocity at the bump (where the gas is deviating in comparison to the surroundings). For the intact holes, we used the average difference between v_{Hel} and the velocities of the gas in the approaching and receding sides of the hole. The uncertainty of the calculation is again the velocity resolution (1.3 or 2.6 km s^{-1}).

We further assigned quality points to the holes according to the following criteria. If the intensity profile interactively displays the center of the hole as stationary across channels then the hole is given one point. A big depression in the intensity profile provides another one point. **We assigned this point by visual inspection.** Additionally, ‘sharp’ edges in the pv diagrams of Type 1 holes provide one point, a velocity deviation (‘bump’) in the intact side of a Type 2 hole provides one point, and if there is a bump of at least 2 channel width, it gets two points.

Finally, we added all the quality points for selection. Following the criteria of Bagetakos et al. (2011), holes with a quality value less or equal to five are discarded. So, from the original list of 1181 possible holes only 306 holes are considered as robust identifications.

3.2. Basic and Calculated Properties

Table 2 lists the basic properties of the galaxies and holes we cataloged for each galaxy. The number of holes per galaxy in our sample ranges from 0 (NGC 4163, VII Zw 403) to 41 (DDO 50), with hole diameters (d) from 38 pc to 2.3 kpc and expansion velocities between 5 and 30 km s^{-1} (recall that expansion velocities for Type 1 holes were not measurable, and so we take the average velocity dispersion in a quiet part of the galaxy as the expansion velocity limit). Nine galaxies contain only Type 1 holes (broken out—neither side visible in the pv diagram) while four galaxies

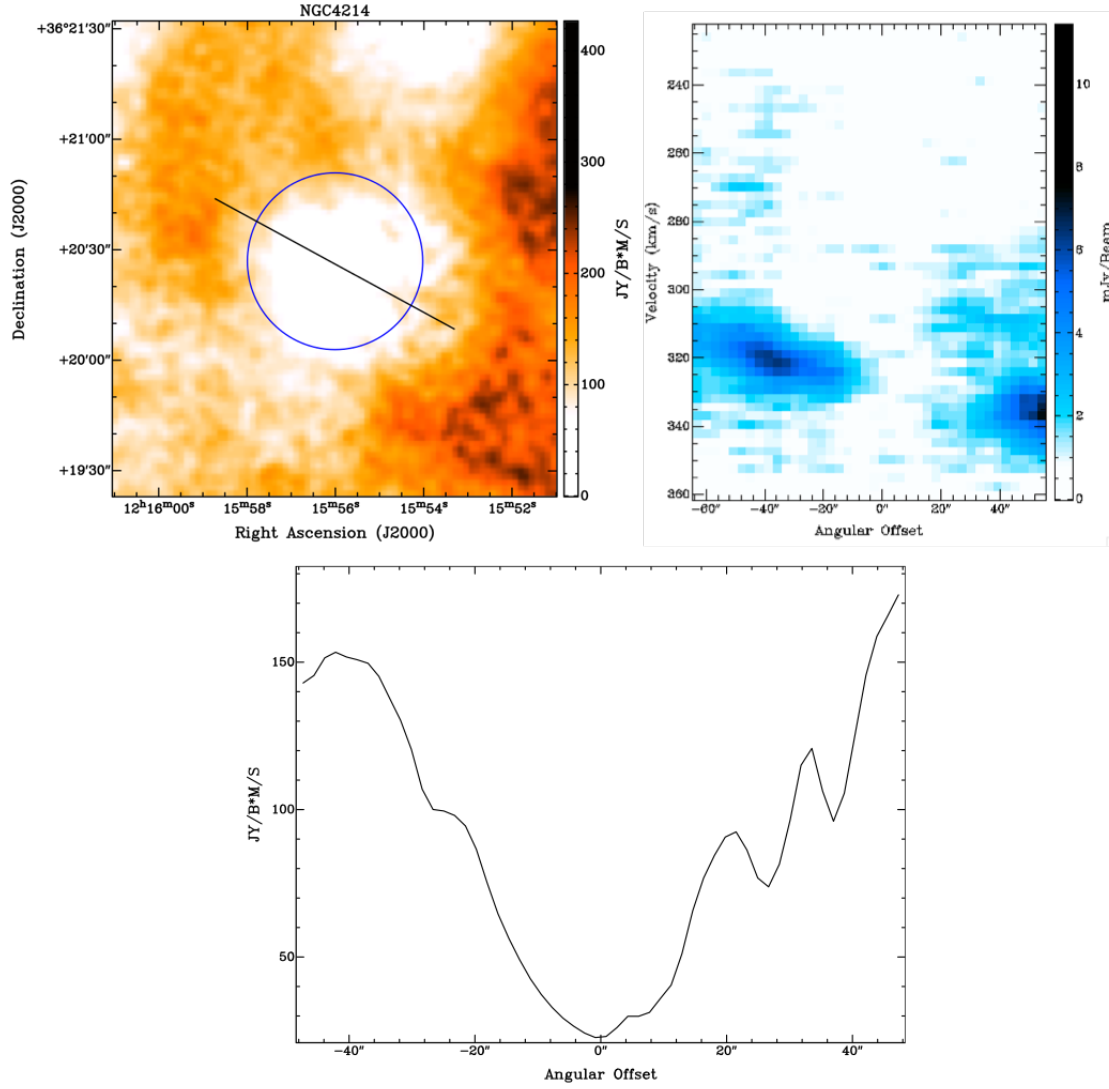


Figure 1. “Hole” in the integrated H I map of NGC 4214 showing ellipse and major axis (upper left); Position-velocity diagram (*pv* slice; upper right) created along the major axis; and intensity profile (bottom) of the hole.

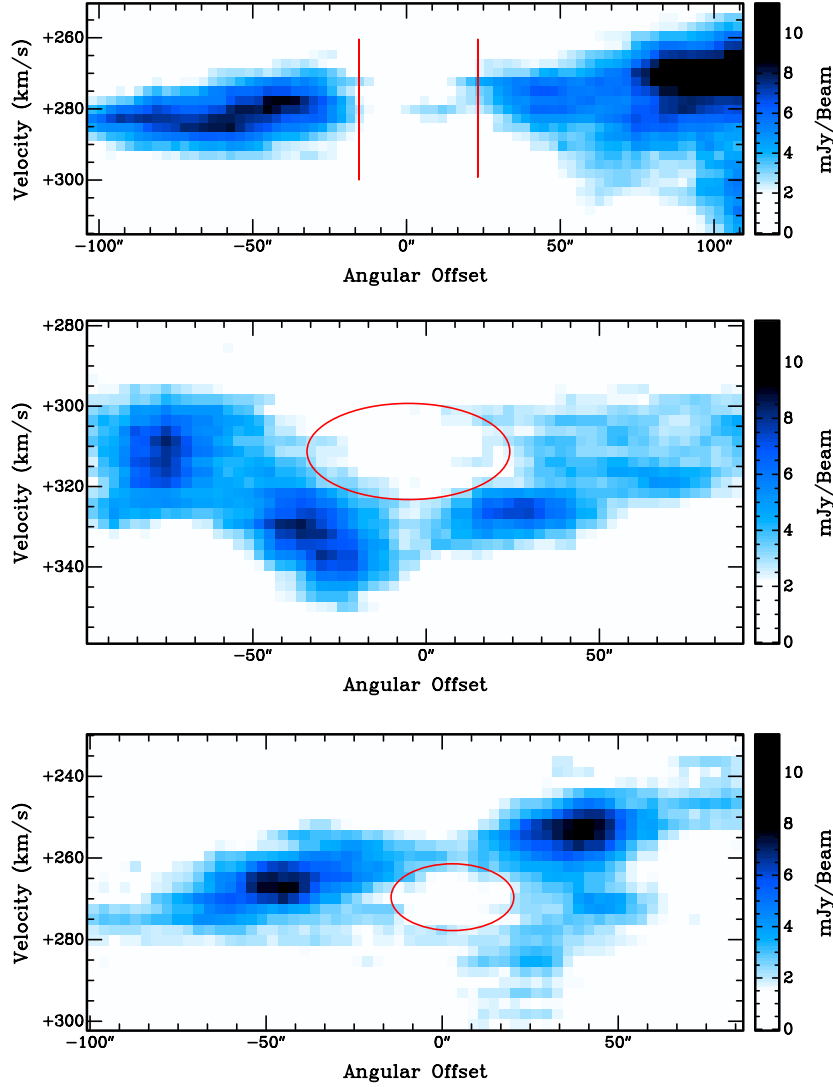


Figure 2. Position-velocity (pv) diagrams of three types of holes (these features are from NGC 4214). Top: Type 1 hole (completely blown out); middle: Type 2 hole (partially blown out); and bottom: Type 3 hole (intact).

contain only Type 3 holes (intact—both sides visible in the pv diagram). We also list the derived properties for each galaxy in Table 2, including the size (radius) of the H I gas disk, R_{max} defined as where the rotation curve ends or stops rising (flattens out) as seen in the pv diagram taken along the galaxy’s major axis. The smallest gas disk we measure is for DDO 187 with $R_{\text{max}} = 0.5$ kpc; the largest is for DDO 50 with $R_{\text{max}} = 6.7$ kpc. The rotation velocities, defined as the velocity at R_{max} , range from 6 km s^{-1} for SagDIG to 77 km s^{-1} for NGC 4214.

The basic properties of the H I holes were used for the following fundamental calculations of the derived properties.

- The kinetic age (t_{kin}) of a hole is calculated by assuming a constant expansion rate v_{exp} throughout its life time as:

$$t_{\text{kin}} = 0.978 \frac{d/2}{v_{\text{exp}}} \quad (1)$$

Table 2. Basic Properties of the Holes in the LITTLE THINGS Galaxies

Galaxies	No. of Holes	Type 1 (%)	Type 2 (%)	Type 3 (%)	v_{exp} (km s ⁻¹)	d (pc)	R_{max} (kpc)	v_{rot} (km s ⁻¹)	v_{disp} (km s ⁻¹)	Z_0 (pc)
CVnIdwA	1	100	0	0	8	248	1.4	19	8	240
DDO 43	15	7	53	40	7 - 16	386 - 797	4.7	33	8	470
DDO 46	18	17	28	55	6 - 15	217 - 743	3.0	74	9	150
DDO 47	19	53	26	21	8 - 15	428 - 1623	6.6	40	9	610
DDO 50	41	61	20	19	8 - 18	181 - 1889	6.7	39	9	630
DDO 52	17	30	35	35	8 - 15	382 - 959	4.9	68	8	240
DDO 53	7	14	0	86	8 - 15	126 - 340	2.4	19	9	470
DDO 63	7	29	29	43	8 - 15	208 - 950	4.0	...	8	...
DDO 69	4	50	50	0	7 - 12	38 - 331	1.0	13	7	230
DDO 70	9	89	11	0	9 - 13	171 - 791	2.3	31	9	280
DDO 75	4	100	0	0	9	269 - 1195	3.7	42	9	330
DDO 87	18	28	39	33	6 - 15	356 - 1821	7.1	45	7	460
DDO 101	2	0	50	50	10 - 16	335 - 355	1.8	72	9	90
DDO 126	4	75	0	25	9 - 12	465 - 996	2.9	36	9	290
DDO 133	5	100	0	0	10	494 - 856	2.4	43	10	230
DDO 154	9	56	22	22	5 - 10	183 - 644	7.1	48	8	480
DDO 155	3	100	0	0	10	225 - 288	0.7	20	10	140
DDO 165	3	33	34	33	12 - 13	347 - 1797	3.0	32	12	460
DDO 167	3	67	0	33	8 - 9	269 - 391	1.0	14	8	240
DDO 168	2	50	0	50	8 - 10	501 - 751	1.9	30	8	210
DDO 187	3	0	33	67	11 - 14	115 - 173	0.5	32	10	60
DDO 210	1	100	0	0	6	79	0.5	11	6	110
DDO 216	3	0	0	100	8 - 9	147 - 320	0.7	17	7	120
F564-V3	8	0	38	62	8 - 15	588 - 1208	2.4	50	7	140
Haro 29	2	0	0	100	11 - 13	405 - 439	2.3	38	9	220
Haro 36	1	0	0	100	18	1137	2.4	76	17	220
IC 10	20	70	25	5	13 - 26	46 - 250	1.5	52	16	190
IC 1613	11	100	0	0	6	143 - 821	2.3	25	6	220
LGS 3	7	57	0	43	5 - 10	27 - 57	0.4	13	5	60
M81dwA	10	10	10	80	7 - 10	183 - 1176	1.8	15	7	340
Mrk 178	1	0	0	100	16	357	0.9	14	10	250
NGC 1569	5	60	20	20	22 - 30	228 - 351	1.8	74	22	220
NGC 2366	11	36	46	18	6 - 15	189 - 632	6.2	69	11	400
NGC 3738	3	100	0	0	18	340 - 399	1.4	...	18	...
NGC 4163	0	0	0	0	0.8	20	9	140
NGC 4214	21	71	19	10	9 - 20	262 - 2334	6.3	77	9	300
SagDIG	1	100	0	0	9	666	1.0	6	9	650
UGC 8508	3	33	0	67	8	117 - 262	1.4	32	8	140
WLM	4	100	0	0	10	102 - 268	0.9	38	10	100
VII Zw 403	0	0	0	0	1.7	40	10	170

where $d = 2\sqrt{b_{\text{maj}} b_{\text{min}}}$ is the diameter of the hole and b_{maj} and b_{min} are the major and minor axes of the hole. The kinetic age, the diameter and the expansion velocity are measured in Myr, pc and km s⁻¹ respectively.

- The effective thickness (l) of neutral hydrogen disk was calculated as

$$l(r) \text{ (pc)} = \frac{Z_0 \sqrt{2\pi}}{\cos i} \quad (2)$$

where i is the inclination of the galaxy and the scale height (Z_0) of galaxies is given by

$$Z_0 \text{ (pc)} = \frac{v_{\text{disp}}}{\sqrt{4\pi G \rho(r)}} \quad (3)$$

with

$$\rho(r) = \frac{3}{4} \frac{M_{\text{dyn}}}{\pi R_{\text{max}}^3}; \quad M_{\text{dyn}} = \frac{v_{\text{rot}}^2 R_{\text{max}}}{G} \quad (4)$$

and the rotational velocity

$$v_{\text{rot}} = \left(\frac{(|v_{\text{rot(max)}} - v_{\text{sys}}| + |v_{\text{rot(min)}} - v_{\text{sys}}|)/2}{\sin i} \right). \quad (5)$$

We averaged out the velocity dispersion value in quiescent parts of the galaxy using the natural-weighted second moment maps to get an average velocity dispersion, and M_{dyn} is the dynamical mass of the galaxy. The systemic velocity (v_{sys}) is the velocity at the center of the sample galaxy, and is a measure of a galaxy's overall motion relative to us. The highest and the lowest values of rotational velocities, i.e., $v_{\text{rot(max)}}$ and $v_{\text{rot(min)}}$ are measured from the natural-weighted integrated H I intensity map and pv diagram of the data cube of the sample galaxy. We estimated $v_{\text{rot(max)}}$ and $v_{\text{rot(min)}}$ using a pv diagram along the major axis, and measured at the points where the velocity rotation curve becomes flat at its maximum and minimum values, and the distances from the center of the galaxy to those points are taken as R_{max} and R_{min} respectively. For galaxies with a face-on ($i = 0^\circ$) inclination, we can't use the H I data to determine ρ and therefore the scale height. Although it's possible to use other methods to estimate the gas and stellar mass surface densities and thus the scale height, we don't do this here to maintain consistency with the rest of the sample.

- The integrated flux density and the major and minor axes (θ_{maj} , θ_{min}) of the synthesized beam are used to calculate brightness temperature (T_{B}) as:

$$T_{\text{B}}(K) = \frac{S \lambda^2 (\text{Jy beam}^{-1} \text{cm}^2)}{2.7 \theta_{\text{maj}} \theta_{\text{min}} (\text{sq. arcmin})} \quad (6)$$

where $1 \text{ Jy} = 10^{-26} \text{ W m}^{-2} \text{ Hz}^{-1}$. From Equation 6, we can write the brightness temperature

$$T_{\text{B}}(K) = \frac{S}{1.66 \times 10^{-3} B_{\text{maj}} B_{\text{min}}} \quad (7)$$

where B_{maj} and B_{min} , measured in arcsec, are the major and minor axes of the beam respectively. S is the mean flux density in mJy beam^{-1} around the hole. The brightness temperature is directly related to H I column density:

$$N_{\text{HI}}(\text{cm}^{-2}) = 1.82 \times 10^{18} \Sigma_i T_{\text{B}}^i dV \quad (8)$$

where i indicates channels with emission. Equations 2, 7 and 8 are used to calculate the mid-plane H I volume density

$$n_{\text{HI}}(\text{cm}^{-3}) = \frac{N_{\text{HI}}}{3.08 \times 10^{18} l(r)}. \quad (9)$$

- The mass of neutral hydrogen gas which is sufficient to fill up the holes was estimated as

$$M_{\text{HI}}(M_{\odot}) = 0.0245 n_{\text{HI}} V \quad (10)$$

with the volume (V) given by

$$V(\text{pc}^3) = \frac{4}{3}\pi\left(\frac{d}{2}\right)^3 \text{ for spherical holes and} \quad (11)$$

$$V(\text{pc}^3) = (2\pi)^{3/2} Z_0 \left(\frac{d}{2}\right)^2 \text{ for distorted holes.} \quad (12)$$

- We calculated the galactocentric distance to the hole (R) as

$$R(\text{pc}) = D [(x'')^2 + (y'')^2]^{\frac{1}{2}} \quad (13)$$

where $D(\text{pc})$ is the distance of the galaxies from the Sun, and x'' and y'' are given by

$$\begin{aligned} x'' &= x \sin \theta + y \cos \theta, \\ y'' &= \frac{y \sin \theta - x \cos \theta}{\cos i}, \\ x &= (\alpha - \alpha_0) \cos \delta_0, \text{ and} \\ y &= \delta - \delta_0. \end{aligned}$$

Here, (α, δ) and (α_0, δ_0) are the coordinates of the center of the hole and the center of the galaxy respectively, and θ is the position angle of the galaxy's major axis.

- The estimate of the energy required to form a hole by stellar winds and/or SNe is calculated by two different methods. In the first method, we followed [Chevalier \(1974\)](#). This gives an estimate of the energy from a single supernova explosion and uses the current expansion velocity (v_{exp}), the diameter of the hole (d) and the volume density of gas (n_0). Since the amounts of other components like He and H_2 are undetermined, n_0 is a lower limit. We replace n_0 by the volume density (n_{HI}) of neutral hydrogen.

$$E_{\text{Ch}}(\text{erg}) = 5.3 \times 10^{43} n_0^{1.12} (\text{cm}^{-3}) \left(\frac{d(\text{pc})}{2}\right)^{3.12} v_{\text{exp}}^{1.4} (\text{km s}^{-1}). \quad (14)$$

The second estimate is based on [McCray & Kafatos \(1987\)](#) which considers multiple explosions of supernovae for the creation of a hole. It is given as:

$$E_{\text{Mc}}(\text{erg}) = n_0 \left(\frac{d(\text{pc})}{194}\right)^2 \left(\frac{v_{\text{exp}}(\text{km s}^{-1})}{5.7}\right)^3 \times 10^{51}. \quad (15)$$

4. ANALYSIS OF THE PROPERTIES

Figure 3 shows the histogram of the radial distribution of the HI holes in each galaxy as a function of relative frequency in percentage. Only a few galaxies, DDO 43, DDO 46, DDO 47, DDO 50, DDO 53, DDO 70, DDO 87, WLM, NGC 3738 and IC 10 have holes at all radial distances. DDO 52, DDO 75, DDO 126, DDO 133, DDO 187, F564-V3 and LGS 3 have more holes in their outskirts, while DDO 63, DDO 154, NGC 2366, NGC 4214 and IC 1613 have more holes in their inner regions. In Figure 4, a histogram of the radial distribution of all the HI holes is plotted. **About 85% of the holes are found within ≈ 0.15 to 0.80 relative radial distance (R/R_{max}) from the center of the galaxies.**

The number distribution of the diameter of the holes of each galaxy is shown in Figure 5. Each panel shows the histogram of the diameter (kpc) of the holes versus its relative frequency in percentage. DDO 47, DDO 50, DDO 87 and NGC 4214 have a wide range of hole sizes. Figure 6, which plots the hole diameters for the entire galaxy sample, shows that approximately 75% of the holes have diameters less than 500 pc. We have only 22 holes larger than a

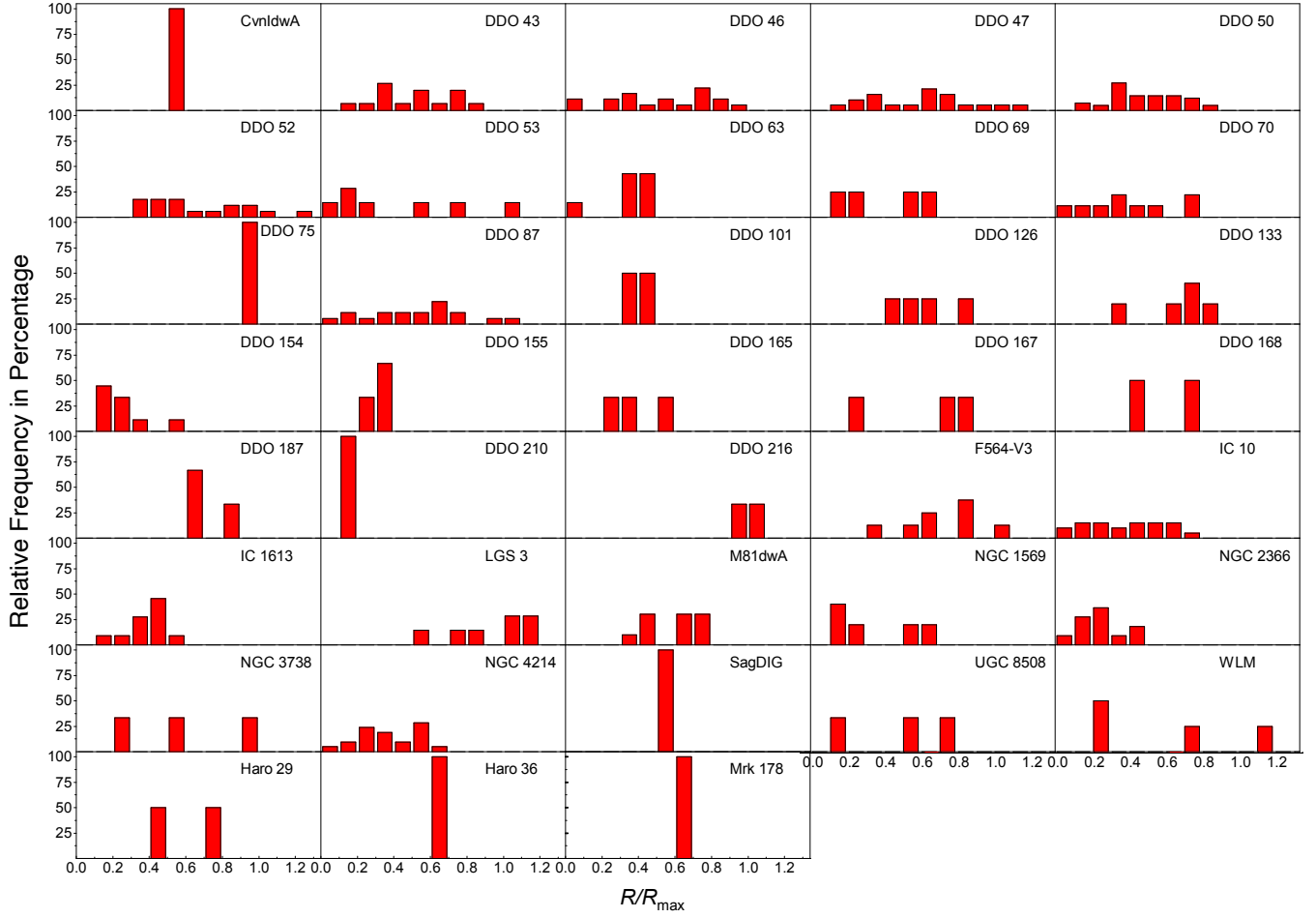


Figure 3. Relative radial distribution of H I holes.

kiloparsec. The size of a hole (and its type) are affected by the overall size and scale height of a galaxy: smaller galaxies and scale heights mean holes will blow out at smaller sizes and possibly younger ages.

Figure 7 shows the location and size of all the holes in the sample relative to the normalized V-band scale length (R_{Sc}) of the galaxies. The plot shows that the concentration of the holes is in between one and two V-band scale lengths.

The distribution of the expansion velocities of the Type 2 and Type 3 holes is given in Figure 8. For some galaxies like DDO 43, DDO 47, DDO 50, DDO 52, DDO 53, F564-V3, LGS 3 and M81dwA, we see a decreasing percentage of holes with higher expansion velocities. **Figure 9 shows the relative number distribution of expansion velocity of Type 2 and Type 3 holes which shows that most of those holes ($\approx 70\%$) are expanding at velocities between 6 to 16 km s⁻¹.** The plot of the expansion velocities of all the holes against their normalized radial positions is in Figure 10. We see that the fastest expanding holes are located more towards the inner/middle parts of the galaxies.

Figure 11 shows the histogram of the distribution of the ages of different types of holes. It shows that most of the Type 2 and Type 3 holes have kinetic ages less than 40 Myr. Ages for Type 1 holes are estimated as an upper limit because the expansion velocity for Type 1 hole is taken as the velocity dispersion of the quiescent area of that galaxy, which is a lower limit.

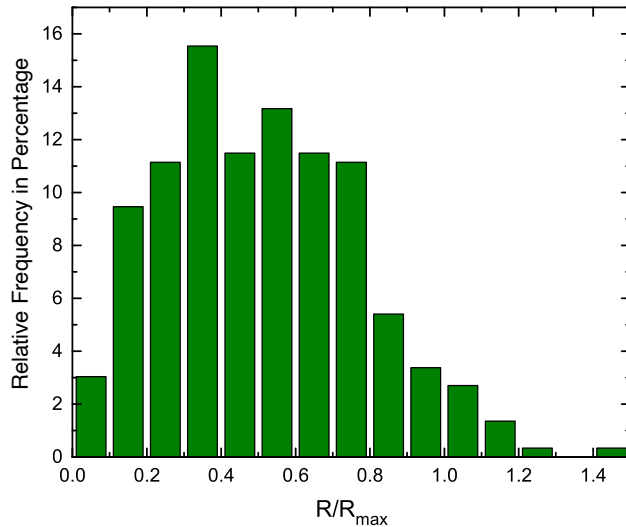


Figure 4. Relative radial number distribution of H I holes for the entire sample.

In Figure 12, we show the percentage of holes per unit area in the inner vs. the outer regions of the galaxies. The dividing line is set by the ‘break radius,’ which is the distance from the center of the galaxy to the point at which the stellar surface brightness profile changes sharply, indicating a change in the stellar distribution (Herrmann et al. 2013). But interestingly, the percentage of holes per unit area inside and outside the V-band break radius is nearly constant.

The percentage distribution of the logarithm of the energy required to form holes (calculated using McCray and Kafatos method (McCray & Kafatos 1987)) is given in Figure 13. From the histograms, we see that there are only a few galaxies having holes which require more than 4×10^{54} ergs of energy (in the entire sample, there are 10 holes which require that energy).

The amount of energy required for the hole formation is plotted with the normalized radial distribution of all the holes in Figure 14. We see the energy required is higher in the inner disk of the galaxies than the outer parts. This might be due to higher gas density and higher star formation rate (SFR) near the center than the peripheral area.

5. POROSITY

Porosity is defined as the ratio of the total area or volume covered by holes to the total area or volume covered by the H I associated with the galaxy (Cox & Smith 1974). Joseph Silk in 1997 first proposed from theory that there should be an anti-correlation between H I porosity and H α surface brightness (star formation) (Silk 1997). Our expectation is that porosity might enhance star formation up to a certain limit. Assuming the holes are formed from stellar feedback, and they are continuously expanding, shells around the holes get thicker and thicker with time, resulting in an increase in temperature and pressure, which ultimately promotes the birth of the next generation of stars. Stellar feedback in the form of ionizing radiation, winds, and supernova explosions from these new born stars again creates holes and hence helps to form another generation of stars. The process goes on until the gas becomes too porous to get collected such that the star formation activity declines from that point i.e., the ISM becomes too porous for star formation to occur. Porosity is calculated in both two and three dimensions for our analysis, and the results are discussed below. The star formation activity is calculated using H α emission and also from FUV emission. **H α emission traces the most recent star formation up to 10 Myr, possibly up to 50 Myr; FUV is from stars formed in the past 100-200 Myr (Bagetakos et al. 2011; Kennicutt & Evans 2012).**

5.1. Surface Porosity

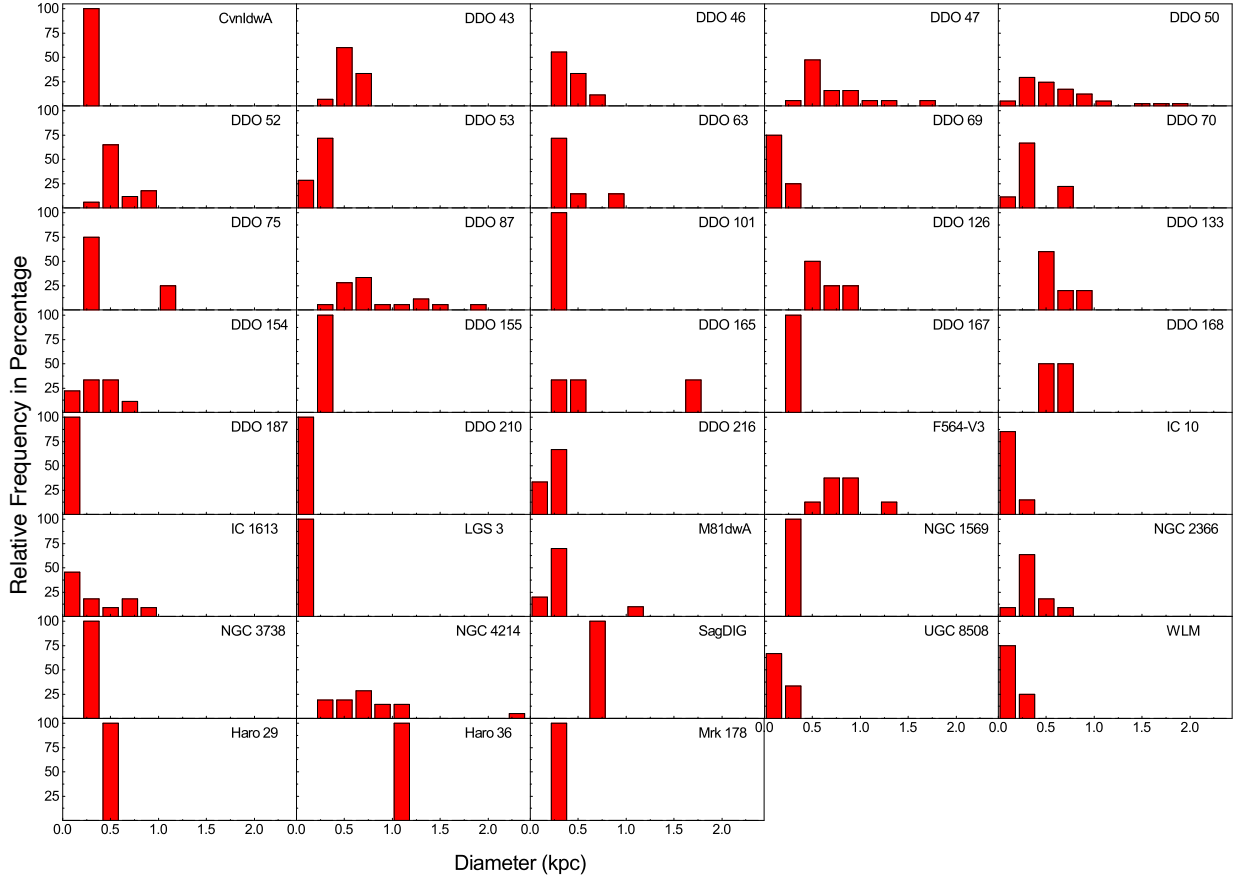


Figure 5. Relative number distribution of the size of the H I holes.

We calculated the ratio of the total area covered by cataloged holes to the total area covered by the H I out to a limiting column density of $5 \times 10^{19} \text{ atoms cm}^{-2}$. This measures the surface porosity (Q_{2D}) of the galaxy. We used AIPS tasks BLANK and ISPEC to estimate the area covered by H I to our column density limit. Calculation shows that most of the LITTLE THINGS galaxies have a surface porosity $\leq 15\%$ (Table 3, Figure 15). The exceptions are M81dwA and F564-V3, with Q_{2D} about 25% and 20% respectively. There are four galaxies in our sample with no H α emission indicating little/no star formation within the past 10 Myr. We found highly porous M81dwA and F564-V3 are two of them. These two galaxies have very low FUV emission as well. Conversely, DDO 210 has very low porosity (0.8%) with no star formation rate calculated from H α emission and the second lowest FUV emission in the sample. LGS 3 also has no H α emission and the lowest FUV emission but its surface porosity is about 7%. Galaxies NGC 1569, NGC 2366, Haro 29, NGC 4163, VIIZw 403, NGC 3738 and IC 10 have very low surface porosity ($\leq 1.6\%$), but have high star formation rates whereas the galaxies NGC 4214 and DDO 50 have high SFR as well as high surface porosity (9% and 11% respectively).

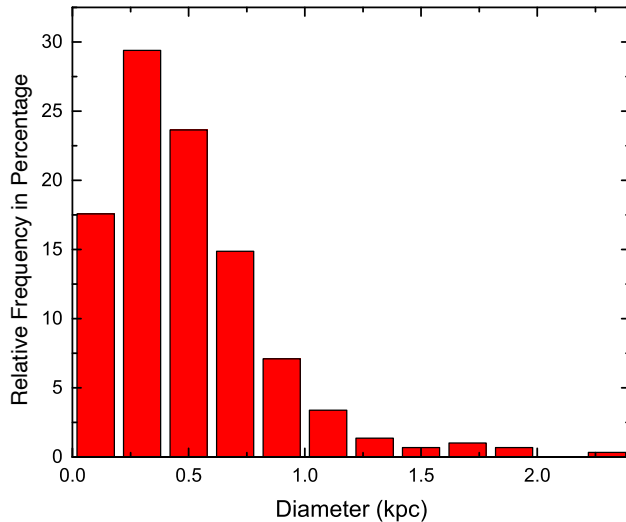


Figure 6. Relative number distribution of the size for the H I holes of entire sample.

5.2. Volume Porosity

For the volume porosity (Q_{3D}), we calculated the ratio of the total volume of holes to that of the galaxy volume. We estimated the volume of the holes assuming they are spherical. For the estimate of the volume occupied by neutral hydrogen, we used the area from the surface porosity calculation and used the estimated scale height as the third dimension. We assumed the scale height is constant throughout the H I disk. The volume porosity of most of the sample galaxies lies within the range $\leq 6\%$ except for F564-V3 ($\approx 9\%$) and M81dwA ($\approx 8\%$) which have no recent star formation (no $H\alpha$ emission). IC 10 has the lowest volume porosity (nearly equal to 0%) among all the sample galaxies followed by CVnIdwA and NGC 1569. Values are given in Table 3 and plotted in Figure 15.

From the results of the relation between the surface and volume porosity with star formation rates as shown in Figure 15, it is clearly seen that there is wide variation in star formation rate at low porosity. However, it is not clear whether high porosity is unfavorable for star formation. According to the $H\alpha$ tracer, two highly porous galaxies have no recent star formation at present; but some star formation is seen in these galaxies using the FUV tracer. Recall that $H\alpha$ and FUV indicate star formation at different ages. $H\alpha$ shows SF in the past 10 Myr, FUV the past 100 to 200 Myr. So perhaps these galaxies had $SF \approx 100$ Myr ago, but are so porous that it shut off, hence no $H\alpha$. For now, this remains speculative.

We don't see any obvious relation between the porosity and star formation, which might have two possible reasons. Either there is no specific correlation between H I porosity and star formation rate or our sample is not large enough to see the correlation.

6. STAR FORMATION RATE AND STAR FORMATION HISTORY

Stellar feedback (supernova explosions and stellar radiation) is considered one of the most probable mechanisms for the origin of H I holes. The idea is that star clusters (such as OB associations) provide sufficient energy from stellar feedback to push out the gases around them which eventually creates a hole and a denser shell around the hole. Continued expansion increases the density and temperature of the shell triggering another generation of stars (Oey & Clarke 1997). This explanation is supported by Gil de Paz et al. (2007) and Thilker et al. (2007, 2008) using the GALEX Nearby Galaxies Survey. Based on this understanding, we expect the amount of energy required to form a hole to correlate with the number and type of stars that produced it. To test this, we estimate the star formation rate needed to form a hole and look for an observational correlation with a star formation tracer such as $H\alpha$.

We estimated the number of total supernovae required to create each hole using the average energy produced during a supernova explosion ($\approx 10^{51}$ erg) as in McCray & Kafatos (1987). We also assumed the lower limit of the lifetime

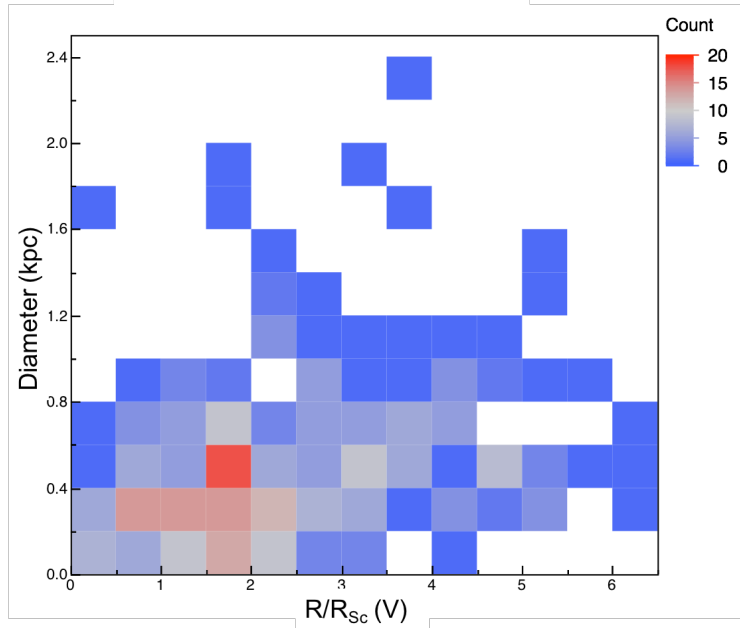


Figure 7. Distribution of H I holes: diameter vs. normalized V-band scale length.

of a hole to be ≈ 60 Myr, and that all the holes are formed by Type II supernovae of stars with masses $\gtrsim 8 M_{\odot}$ (Bagetakos et al. 2011). However, the holes may persist a long time in a dwarf after expansion stops due to lack of rotational shear.

The plot of the number of supernovae required to form the holes versus the kinetic age of the holes for 36 LITTLE THINGS galaxies is shown in Figure 16 which shows the kinetic age of the holes versus the number of supernovae (SNe) required to form each hole. **In the figure, the holes are shown only up to 50 Myr. The remaining 17 holes (most of them are Type 1 holes) with age older than 50 Myr are included in hole properties tables in Appendix B.** To calculate the number of SNe, we have used 10^{51} erg (McCray & Kafatos 1987) as the average energy released by one supernova. There is no observed correlation between age and number of SNe, but this plot also provides a rough estimate of the star formation history of each galaxy if we assume the H I structures were created by star formation. As we see, DDO 69, DDO 187, IC 10, NGC 1569 and WLM have very recent star formation activities, ≈ 10 Myr or less. For some of the galaxies like DDO 46, DDO 50, NGC 2366, and NGC 4214, the SFH is more or less constant throughout the period.

Using the supernova history estimated from the holes, we can estimate the supernova rate (SN rate). We calculated the SN rate for each hole using the current expansion velocity, the radius of the hole, and the number of supernovae required to form the holes. The SN rate is proportional to the star formation rate (SFR) for stars with masses $\gtrsim 8$

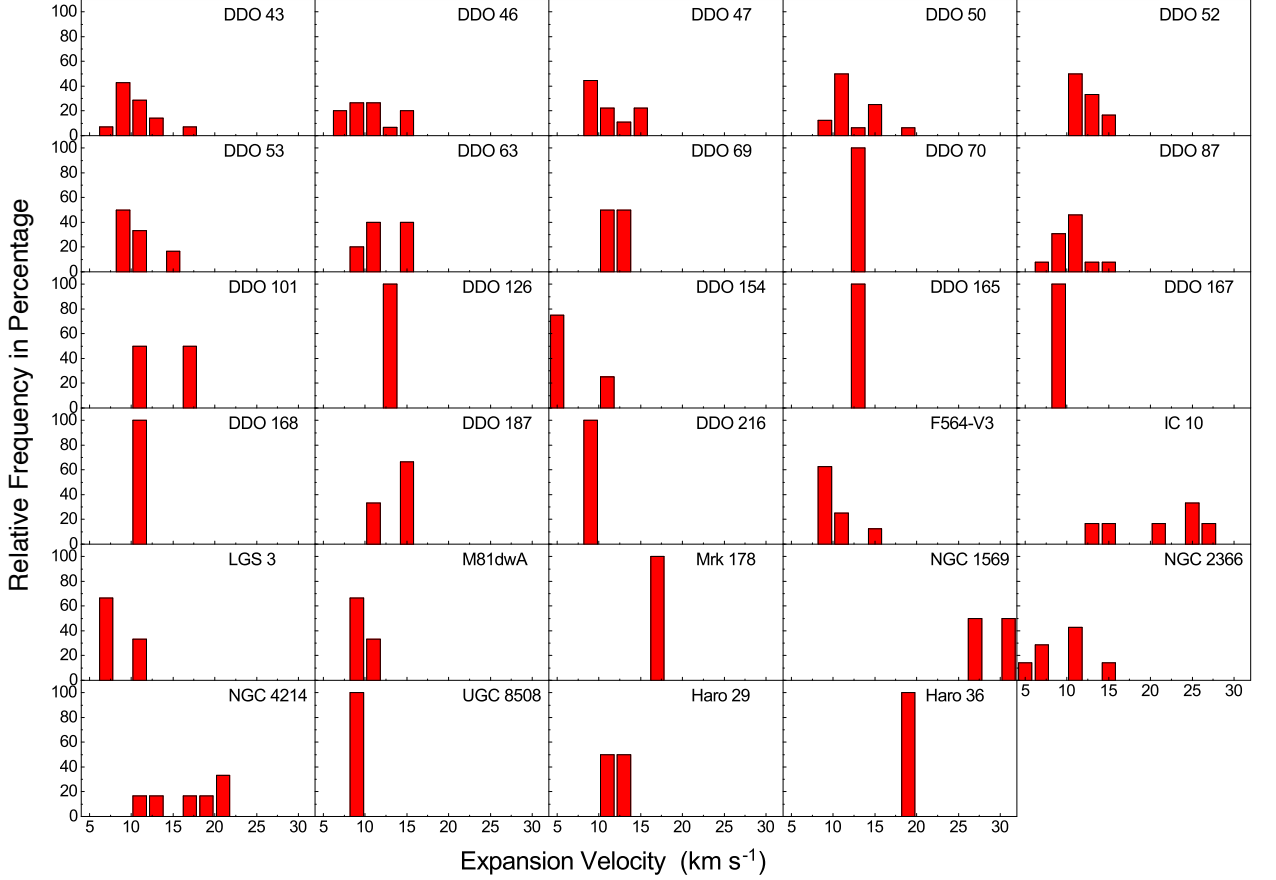


Figure 8. Relative number distribution of the expansion velocity of Type 2 and Type 3 holes.

M_{\odot} . The constant of proportionality is calculated by integrating the Salpeter initial mass function

$$N = \int_{0.1}^{120} A M^{-2.35} dM, \quad (16)$$

where A is the constant of proportionality, M is the mass of the star, and N is the number of stars formed. The stellar mass limits (0.1 to $120 M_{\odot}$) are taken as in [Bagetakos et al. \(2011\)](#). We find the relation between the total SFR (including stars with masses less than $8 M_{\odot}$) and the SFR as estimated from the number of SNe required to create the holes as

$$\text{SFR}_{\text{Holes}} \approx 134 \text{ SFR} (M_{\odot} \gtrsim 8). \quad (17)$$

Since the hole formation process is ongoing and we are calculating the star formation rate from the holes using their properties, the calculated value of $\text{SFR}_{\text{Holes}}$ gives the lower limit of the star formation rate. Note that the upper limit of the age of the holes used in the calculation underestimates the $\text{SFR}_{\text{Holes}}$. The calculated values of SFR from the holes are in Table 3.

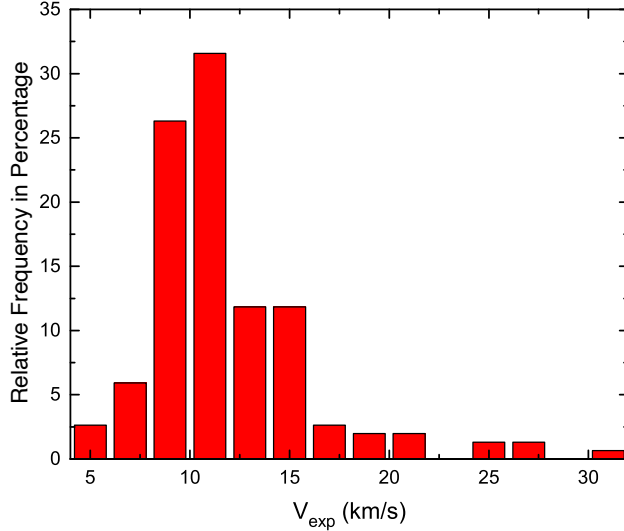


Figure 9. Relative number distribution of the expansion velocity of Type 2 and Type 3 holes for the entire sample.

We can now test whether the star formation activity required to form the holes is consistent with the amount of recent star formation as indicated by $\text{H}\alpha$ and FUV emission. **The star formation rates from $\text{H}\alpha$ and FUV are taken from Hunter & Elmegreen (2004) and Hunter et al. (2010) respectively. Extinction is considered while estimating the SFR from both $\text{H}\alpha$ and FUV flux.** In Figure 17, the star formation rate estimated from the holes is plotted with the star formation rates measured from $\text{H}\alpha$ and FUV data. In general, the relation shows that the holes are consistent with being from star formation.

7. CONCLUSION

In this work, we adopted a systematic and consistent procedure to identify and catalog H I holes in dwarf irregular galaxies, and analyzed their properties. This is part of the work of the LITTLE THINGS project which studies 41 nearby dwarf galaxies including 4 blue compact dwarfs.

We searched for holes in the integrated natural-weighted and robust-weighted H I flux density maps and data cubes using the KARMA visualization software and performed a visual inspection following specific criteria. Our initial catalog contains more than 1000 candidate holes. From those structures we selected 306 high quality H I holes. We measured their observed properties and calculated various others, such as the kinetic ages of the holes, the displaced H I mass, the energy required to form those structures, and other properties.

We could measure the expansion velocity of the Type 2 and Type 3 holes, which ranges from 5 to 30 km s^{-1} . The expansion rates of Type 1 holes are not measurable because they are completely broken in position-velocity diagrams. The rotation velocities range from 6 km s^{-1} for SagDIG to 77 km s^{-1} for NGC 4214. The extent of the gas disk is defined as the radius at which the rotation curve reaches a maximum, then drops slightly (perhaps due to a warp) and reaches a plateau extending well beyond the “maximum in the pv diagram”. The smallest gas disk measured from the pv diagrams along the major axis, is for DDO 187 with $R_{\text{max}} = 0.5$ kpc; the largest is for DDO 50 with $R_{\text{max}} = 6.7$ kpc. The estimated H I scale heights of the galaxies range from 60 pc to 650 pc. Most of the holes are midway in the disks of the galaxies, with diameters $\lesssim 0.5$ kpc. However, the Type 1 holes are radially extended in comparison to the Type 2 and Type 3 holes which is consistent with Bagetakos et al. (2011).

Using information from the catalog, we calculated the surface (Q_{2D}) and volume (Q_{3D}) porosities of the H I gas, as defined by the percentage of the surface area (or volume) of the H I content of the galaxy containing holes. From the study of porosity we found that most of the galaxies have $Q_{2D} \leq 15\%$ and $Q_{3D} \leq 6\%$. The four galaxies with no recent SF as measured by $\text{H}\alpha$ have either very low, or very high porosities. Galaxies with low-to-intermediate porosities exhibit a wide range of star formation activity, however.

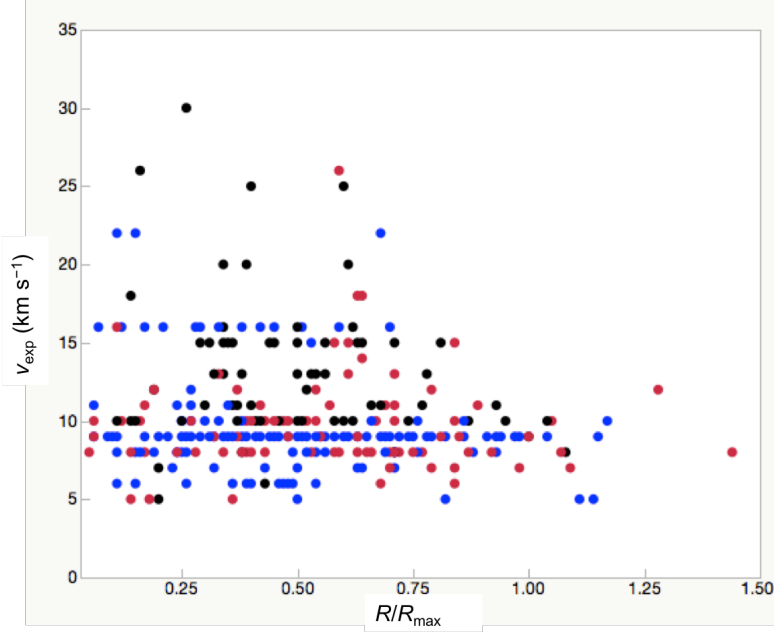


Figure 10. Distribution of H I holes: Expansion velocities with respect to the location. Blue colored points are the upper limits of expansion velocities for Type 1 holes, black and red are the expansion velocities of Type 2 and Type 3 holes respectively.

We do not find a distinct level of porosity that corresponds to a cut-off in star formation as predicted in [Silk \(1997\)](#). It may be that our sample is too small to definitively detect any SF cut-off at high porosities. However, the two galaxies with the highest porosities and no recent SF (but low levels of intermediate-age SF) are consistent with the idea that at some point, the H I becomes too full of holes to support new regions of star formation.

These results are also consistent with the relation we find between the star formation rate estimated from the energy required to create a hole (from SNe, and therefore related to SF) and the star formation rates measured from H α and FUV. This indicates that the holes are consistent with a star formation origin. From this result, we conclude that stellar feedback can be considered as a factor in creating H I holes, as postulated by [Weaver et al. \(1977\)](#); [Cash et al. \(1980\)](#); [Ott et al. \(2001\)](#); [Weisz et al. \(2009b\)](#); [Cannon et al. \(2011\)](#). However, the uncertainty seen in the plots shown in our work support a more complex idea of the relation between star formation and the atomic gas in small galaxies. It may be possible that these structures formed because of the combined result of two or more phenomena such as stellar feedback, turbulence, thermal and gravitational instabilities, gamma ray bursts and/or high velocity cloud impacts, as suggested by the numerical simulations of [Dib & Burkert \(2005\)](#); [Vorobyov & Basu \(2005\)](#).

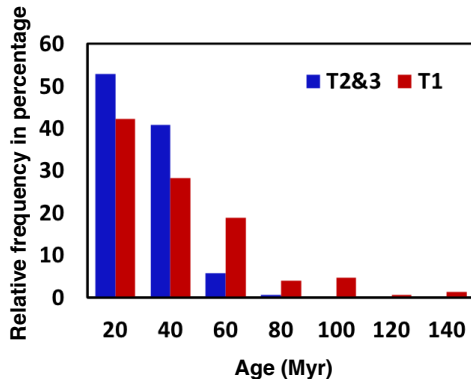


Figure 11. Distribution of the kinetic ages of H I holes.

ACKNOWLEDGEMENTS

This project was funded in part by the National Science Foundation under grant numbers AST-0707563 AST-0707426, AST-0707468, and AST-0707835 to Deidre A. Hunter, Bruce G. Elmegreen, Caroline E. Simpson, and Lisa M. Young. The LITTLE THINGS team is grateful to National Radio Astronomy Observatory for telescope time, for support of team and public data access. The National Radio Astronomy Observatory is a facility of the National Science Foundation operated under cooperative agreement by Associated Universities, Inc. We would like to thank Dr. Elias Brinks for his valuable suggestions and help with this project.

APPENDIX

A description of all the LITTLE THINGS galaxies, H I structures and their properties are presented in the following Appendices.

A. DESCRIPTION OF LITTLE THINGS GALAXIES AND THEIR PROPERTIES

A.1. *CVnIdwA*

Canes Venatici I dwarf A (CVnIdwA) or UGCA 292 is an extremely metal-poor dwarf galaxy [van Zee \(2000\)](#) in the Canes Venatici constellation. The galaxy is situated about 3.6 Mpc away from the Milky Way with V-band magnitude -12.4 , and has only one hole: a Type 1 hole of diameter ≈ 288 pc. The estimated H I disk length and the scale height of the galaxy are about 1.4 kpc and 240 pc respectively.

A.2. *DDO 43*

DDO 43 (PGC 21073, UGC 3860) is located 7.8 Mpc away in the Ursa Major constellation. Although it is a member of the NGC 2841 Group, it is relatively isolated from the other members. Our estimate of the scale height is about 470 pc. [Simpson et al. \(2005b\)](#) identified four apparent H I holes in the ISM of this galaxy. We detected 15 holes with most of them being Type 2 and Type 3. We found only one Type 1 hole which is the largest hole (also the largest hole in [Simpson et al. \(2005b\)](#)) in the galaxy.

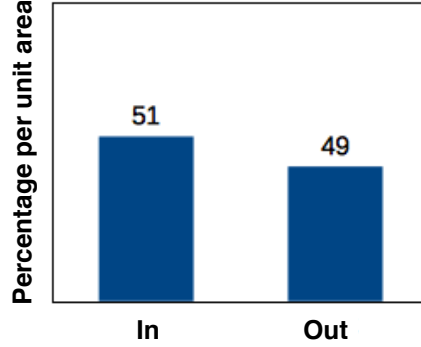


Figure 12. Distribution of H I holes per unit area inside and outside of the break radius.

A.3. DDO 46

DDO 46 (PGC 21585, UGC 3966) is situated 6.1 Mpc away with V-band magnitude -14.7 . The galaxy has 18 H I holes and more than 50% of those holes are Type 3. The estimated scale height and H I disk length are about 150 pc and 3 kpc respectively.

A.4. DDO 47

DDO 47 (PGC 21600, UGC 3974) is an isolated gas-rich dwarf about 5.2 Mpc away. It has 19 holes, about half of which are Type 1, including a supershell (No. 15), which were found in the previous study done by [Walter & Brinks \(2001\)](#). However, we detected another large hole (No. 4) which is not in their list. Our estimate of the scale height of DDO 47 is 610 pc.

A.5. DDO 50

DDO 50 or Holmberg II, also known as UGC 4305, PGC 23324 and VIIZw 223, is one of the largest dwarf galaxies in the LITTLE THINGS sample. It is an M81 Group galaxy with V-band magnitude -16.6 , located at a distance of about 3.4 Mpc. Previous studies of H I holes in DDO 50 done by [Puche et al. \(1992\)](#) detected 51 holes, whereas [Bagetakos et al. \(2011\)](#) restricted the number of holes to 39. The location and size of most of those holes are comparable in both papers. Our hole search resulted in 41 holes in DDO 50. For consistency, we compared the properties of each structure with [Bagetakos et al. \(2011\)](#) and we found that our result is in nice agreement, but we still have fewer holes than [Puche et al. \(1992\)](#) probably because of our selection criteria. Some of the holes in [Puche et al. \(1992\)](#) are considered as a large single hole in our list.

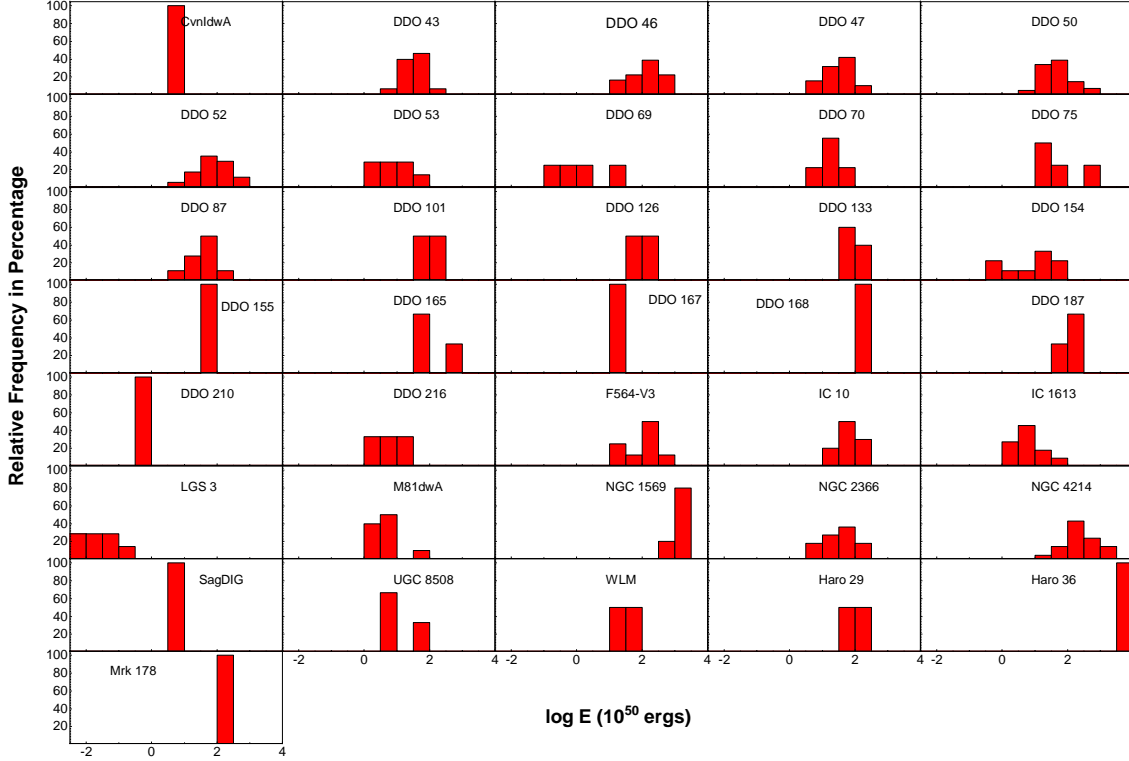


Figure 13. Relative number distribution of the estimated energy required to form H I holes.

A.6. DDO 52

DDO 52 (PGC 23769, UGC 4426), which lies about 10.3 Mpc away, is the most distant galaxy in the LITTLE THINGS sample. It is an isolated galaxy in the NGC 2841 Group (NED⁴). The calculated scale height of the galaxy is about 240 pc, and the H I disk extends to ≈ 4.9 kpc from the galactic center. We detected 17 H I holes in the disk according to our selection criteria.

A.7. DDO 53

DDO 53 (PGC 24050, UGC 4459, VIIZw 238) is another M81 Group member located 3.6 Mpc away with V-band magnitude -13.8 . We found a Type 1 hole and six Type 3 holes in the galaxy which is more than double the number detected by Bagetakos et al. (2011). The estimate of the scale height of the galaxy is 470 pc.

A.8. DDO 63

DDO 63 (Holmberg I, UGC 5139, PGC 27605) is also a member of the M81 Group, located at a distance of 3.9 Mpc, and dominated by a large Type 1 hole. The first detailed study of the H I structure was done by Ott et al. (2001) who discovered one large hole. Later, Bagetakos et al. (2011) found six holes, and our analysis resulted in finding seven holes in the galaxy including the large hole first discovered by Ott et al. (2001). Our estimate of the properties of the

⁴ The NASA/IPAC Extragalactic Database (NED) is operated by the Jet Propulsion Laboratory, California Institute of Technology, under contract with the National Aeronautics and Space Administration.

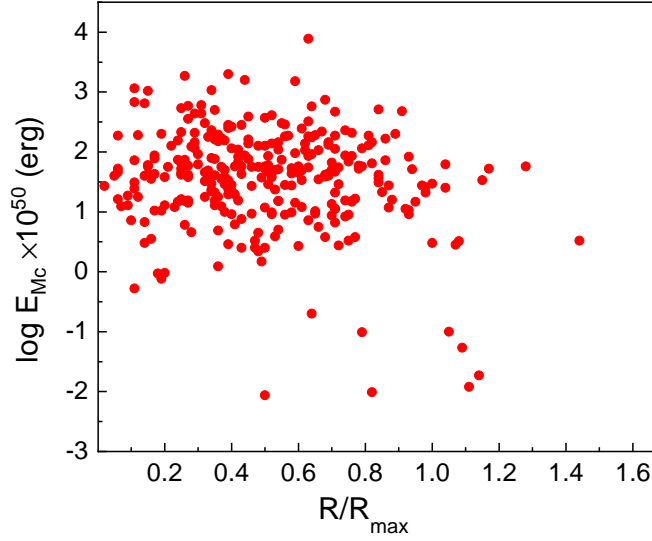


Figure 14. Estimated energy required to form H I holes of the entire sample with respect to their radial distributions.

holes are in good agreement with both previous studies. The scale height and other properties that depend on the scale height were not estimated for this galaxy due to its face-on ($i = 0^\circ$) inclination, as discussed in Section 3.2.

A.9. DDO 69

DDO 69 (PGC 28868, UGC 5364, Leo A) is a Local Group galaxy and Milky Way satellite. It is 0.8 Mpc away with V-band magnitude -11.7 . The galactic disk is dominated by a Type 1 hole (No. 4), and the rest of the holes are quite small in size. The H I disk of the galaxy extends to ≈ 1 kpc.

A.10. DDO 70

DDO 70 (UGC 5373, PGC 28913), most commonly known as Sextans B, is one of the most distant members of the Local Group of galaxies. It is situated ≈ 1.3 Mpc away from the Milky Way in the Sextans constellation. The galactic disk has nine H I holes, and eight of them are Type 1.

A.11. DDO 75

DDO 75, UGCA 205 or Sextans A is located at a distance of 1.3 Mpc from the Milky Way as an isolated member of the Local Group. In V-band light it appears square shaped with magnitude -13.9 . Most of the central portion of the H I disk of this galaxy is dominated by a large Type 1 hole (No. 2). It also has three smaller Type 1 holes, two of which are in the rim of the larger hole, and the last one is in the outskirt of the disk. The estimated scale height of the galaxy is ≈ 330 pc.

A.12. DDO 87

DDO 87 (PGC 32405, UGC 5918) has 18 distinct H I holes in its ISM. It contains all three types of the holes almost in equal proportions. The Type 1 holes of the galaxy are larger than the others and are found in the outer part of the disk. Among them, the diameters of five of the holes are larger than one kiloparsec. The scale height of DDO 87 is estimated to be about 460 pc and the H I disk radius is estimated as 7.1 kpc. This galaxy is situated about 7.7 Mpc away in the M81 Group and in V-band, it has a magnitude of -15 .

A.13. DDO 101

DDO 101 (PGC 37449, UGC 6900) is in the NGC 4062 Group at a distance of 6.4 Mpc with a V-band magnitude of -15 . The H I disk of the galaxy extends to ≈ 1.8 kpc. The galaxy contains two holes, one partially broken and another intact.

Table 3. Porosity and Star Formation Rate

Galaxies	Q_{2D}	Q_{3D}	$\log \text{SFR}_{H\alpha}$	$\log \text{SFR}_{FUV}$	$\log \text{SFR}_{Hole}$	SN per	% of Holes per	% of $H\alpha$ in
	(%)	(%)	($M_{\odot} \text{ yr}^{-1}$)	($M_{\odot} \text{ yr}^{-1}$)	($M_{\odot} \text{ yr}^{-1}$)	Galaxy	unit area in R_{br}	diffused gas
CVnIdwA	0.50	0.03	-2.64	-2.47	-4.11	35	0	...
DDO 43	6.54	0.53	-2.12	-1.83	-1.95	4990	59	44
DDO 46	5.69	2.57	-2.35	-1.85	-1.34	20620	79	56
DDO 47	7.59	1.32	-1.98	-1.63	-1.64	10237	78	59
DDO 50	10.89	2.48	-1.25	-0.97	-1.04	40779	...	37
DDO 52	5.60	2.44	-2.53	-1.83	-1.37	19017	65	...
DDO 53	3.44	0.12	-2.28	-2.12	-2.70	895	91	29
DDO 63	3.33	...	-2.23	-1.89	77	...
DDO 69	4.49	0.38	-3.95	-3.17	-3.86	62	93	53
DDO 70	9.39	3.20	-3.01	-2.39	-2.81	689	0	47
DDO 75	7.71	3.11	-2.21	-1.98	-1.90	5686	0	51
DDO 87	12.35	4.25	-2.35	-1.95	-1.73	8360	86	45
DDO 101	1.92	0.90	-2.55	-2.37	-3.03	416	100	77
DDO 126	5.58	2.11	-2.07	-1.83	-2.56	1227	0	37
DDO 133	5.74	2.67	-2.26	-1.93	-2.48	1490	100	43
DDO 154	1.32	0.08	-2.56	-1.91	-2.71	866	0	45
DDO 155	5.63	2.13	-2.67	...	-4.03	42	85	45
DDO 165	8.51	3.04	-2.48	...	-2.86	612	87	73
DDO 167	7.53	0.72	-2.88	-2.41	-3.60	112	52	42
DDO 168	1.06	0.49	-2.02	-1.72	-2.92	535	0	52
DDO 187	1.98	0.78	-3.64	-2.97	-2.79	729	0	66
DDO 210	0.81	0.04	-7.00	-3.75	-6.60	0
DDO 216	5.26	1.71	-4.19	-3.25	-3.76	78	100	80
F564-V3	19.72	9.18	-7.00	-2.85	-2.38	1855	0	...
Haro 29	1.30	0.15	-1.41	-1.68	-2.72	861	75	6
Haro 36	3.96	1.85	-1.80	-1.37	-1.91	5553	0	...
IC 10	1.54	0.00	-1.62	...	-1.40	17761	89	45
IC 1613	13.05	5.02	-2.61	-2.02	-3.11	346	68	...
LGS 3	7.14	0.33	-7.00	-4.85	-4.65	10	17	...
M81dwA	24.56	8.41	-7.00	-2.94	-3.19	287	0	...
Mrk 178	3.85	0.34	-2.14	-2.12	-3.63	105	0	25
NGC 1569	0.48	0.04	-0.22	-0.49	-1.32	21600	84	51
NGC 2366	1.04	0.07	-0.97	-0.98	-1.95	5079	98	12
NGC 3738	1.26	...	-1.45	-1.25	48	30
NGC 4214	8.55	3.66	-0.85	-0.86	-1.06	39125	86	44
SagDIG	8.60	0.54	-3.8	-2.89	-5.18	3	0	...
UGC 8508	1.81	0.17	-2.78	...	-3.35	198	84	46
WLM	0.58	0.18	-2.84	-2.14	-2.84	644	35	43

A.14. DDO 126

DDO 126 (UGC 7559, PGC 40791) lies about 4.9 Mpc away from the Milky Way in the Canes Venatici I Group and has a V-band magnitude of -14.9 . The galaxy has one Type 3 hole and three Type 1 holes including one kiloparsec-sized hole. The estimated H I disk radius and the scale height of the galaxy are about 2.9 kpc and 290 pc respectively.

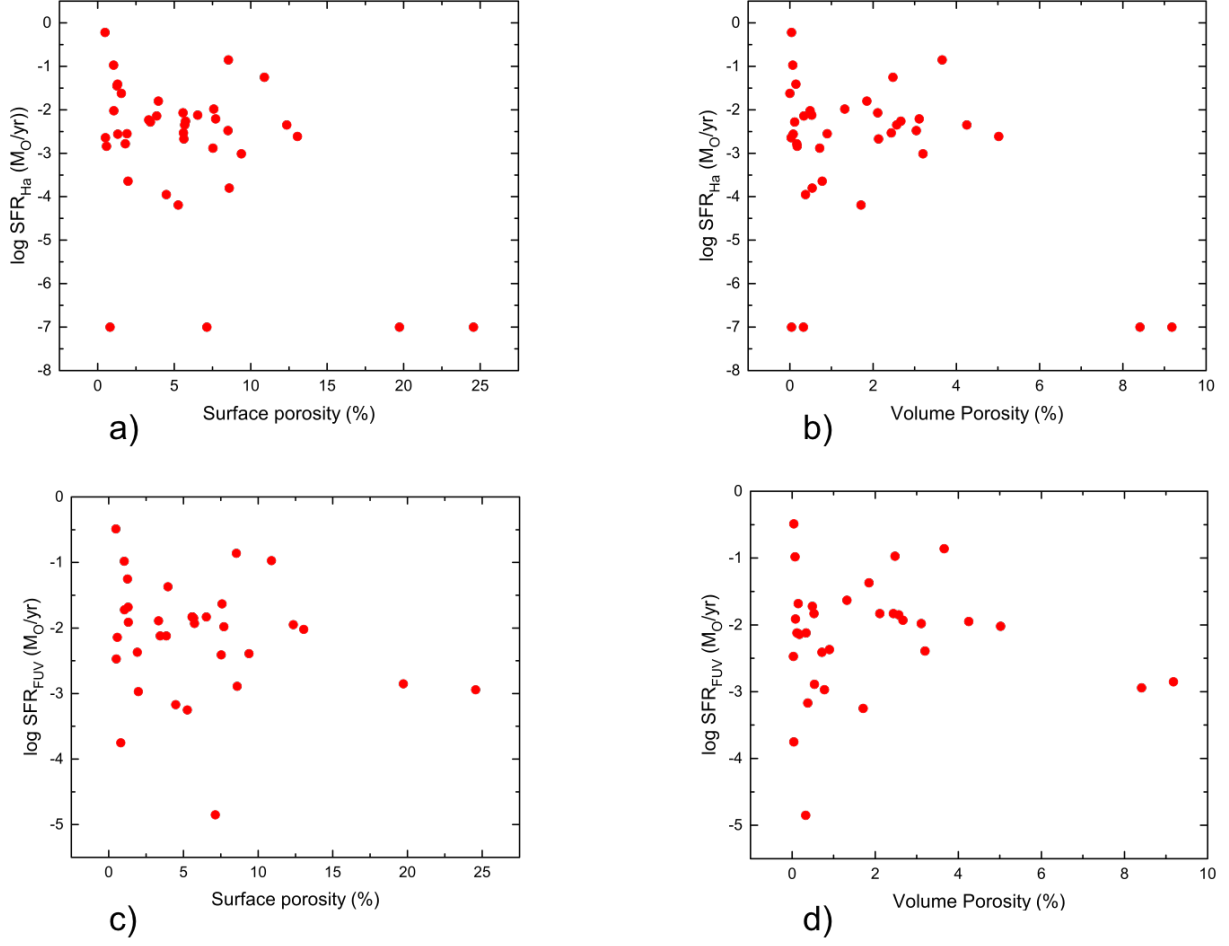


Figure 15. Porosity vs. star formation rate: a) surface porosity vs. the SFR calculated from $\text{H}\alpha$ emission, b) volume porosity vs. the SFR calculated from $\text{H}\alpha$ emission, c) surface porosity vs. the SFR calculated from FUV emission, and d) volume porosity vs. the SFR calculated from FUV emission. In Figures a and b, there is no star formation in the bottom four galaxies; $\text{SFR} = -7$ is assigned just for plotting purposes.

A.15. DDO 133

DDO 133 (PGC 41636, UGC 76980) is situated at a distance of 3.5 Mpc in the Canes Venatici I Group. Its V-band magnitude is -14.8 . DDO 133 has five holes in the ISM, and all are Type 1 holes.

A.16. DDO 154

DDO 154, also known as PGC 43869, UGC 8204 and NGC 4789A, is 3.7 Mpc away from us with a V-band magnitude of -14.2 in the Canes Venatici I Group (Kaisin & Karachentsev (2008)). An earlier study done by Hoffman et al. (2001) found two holes and Bagetakos et al. (2011) found nine holes. We also detected nine holes with the majority being of Type 1. Among LITTLE THINGS galaxies, DDO 154 has one of the largest H I disk sizes ($R_{\text{max}} = 7.1$ kpc).

A.17. DDO 155

DDO 155, Gr 8, LSBC D646-07, PGC 44491 or UGC 8091 has three completely broken holes in its H I disk with two of them overlapping. We estimated the scale height of the galaxy about 140 pc and the disk radius about 0.7 kpc. This galaxy is located in the Local Group at a distance of about 2.2 Mpc.

A.18. DDO 165

DDO 165 (Mailyan 82, PGC 45372 or UGC 8201) is an M81 Group dwarf at a distance of 4.6 Mpc with a V-band magnitude of -15.6 . Cannon et al. (2011) detected seven H I holes in DDO 165. According to our criteria, we have

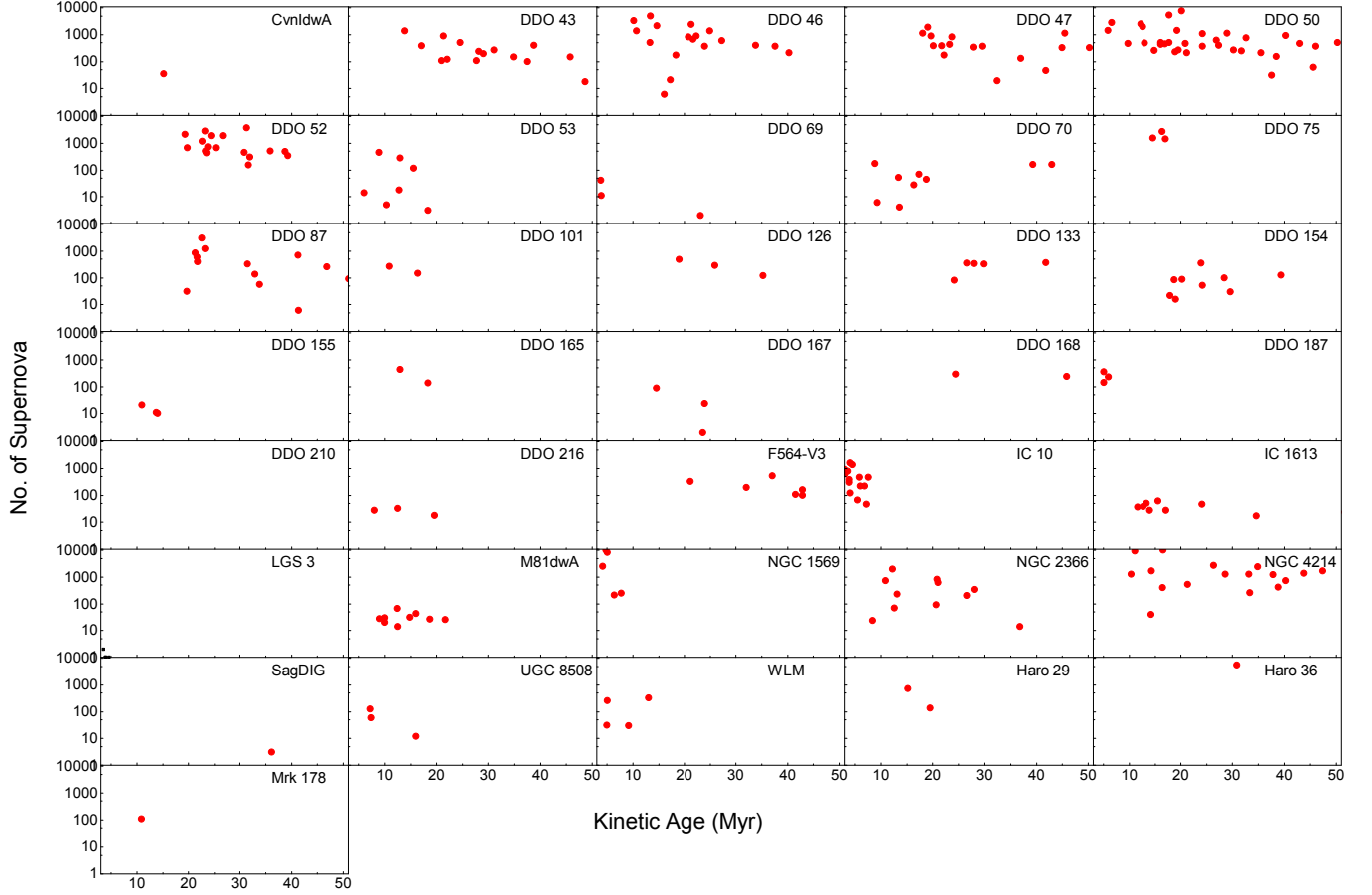


Figure 16. Kinetic age of the H I holes vs. the number of supernovae required to form them.

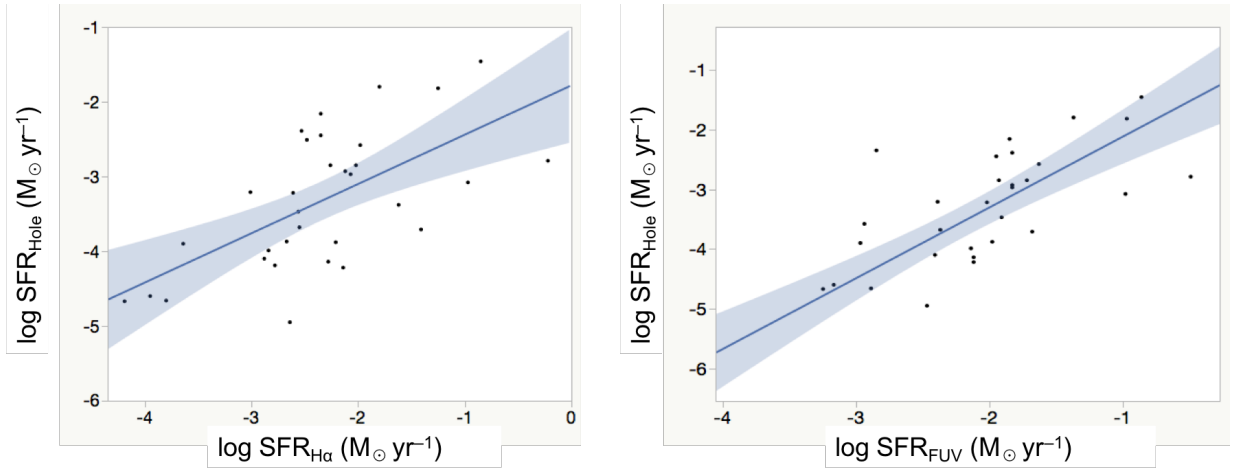


Figure 17. The star formation rate estimated from the energy required to form the H I holes vs. the stellar star formation rates H α (left) and FUV (right). The solid line is the best fit linear regression line. The shaded region shows the confidence limits (95%) for the expected value.

only three ‘good quality’ holes, one of each type. The largest hole we found is in agreement with Cannon et al. (2011) whereas the other two holes are listed by them as a single hole.

A.19. *DDO 167*

DDO 167, also known as PGC 45939 or UGC 8308 lies in the Canes Venatici I group about 4.2 Mpc away. The galaxy has two Type 1 holes and a Type 3 hole in the H I disk which extends to ≈ 1 kpc. The estimated H I scale height of the galaxy is about 240 pc.

A.20. *DDO 168*

DDO 168 (PGC 46039, UGC 8320) is another Canes Venatici I group member also known as PGC 46039 and UGC 8320. It is located 4.3 Mpc away with V-band magnitude -15.7 . The galaxy has two holes, both located in the northern part of the H I disk. The H I scale height of the galaxy is estimated as 210 pc.

A.21. *DDO 187*

DDO 187 (PGC 50961, UGC 9128) is one of the smallest galaxy in the sample in terms of H I disk radius. It has three holes and two of them (Nos. 2 and 3) are overlapped. The galaxy is at a distance of 2.2 Mpc from the Milky Way with a V-band magnitude of -12.7 . We estimated the scale height and the size of the H I disk to be about 60 pc and 0.5 kpc respectively.

A.22. *DDO 210*

DDO 210 is also known as PGC 65367 or the Aquarius Dwarf. It is a relatively isolated member of Local Group situated about 0.9 Mpc away with a V-band magnitude of -10.9 . The galaxy has one small Type 1 hole of diameter ≈ 79 pc. We estimated the scale height about 110 pc and the rotational velocity about 11 km s^{-1} .

A.23. *DDO 216*

DDO 216 (Peg DIG, Pegasus Dwarf, UGC 12613 or PGC 71538) is another Local Group dwarf at a distance of 1.1 Mpc. The galaxy is a companion of Andromeda and lies in the Pegasus constellation. It is one of the smallest galaxies in the LITTLE THINGS group with H I disk radius about 0.7 kpc. The galaxy has three Type 3 holes.

A.24. *F564-V3*

F564-V3 or LSBC D564-08 is situated at a distance of about 8.7 Mpc away from the Milky Way with V-band surface brightness -14 . We detected eight H I holes in this galaxy, five of which are Type 3 and the rest of which are Type 2. The scale height of the galaxy is ≈ 140 pc and the H I disk is extended to about 2.4 kpc.

A.25. *Haro 29*

Haro 29 is a starburst blue compact dwarf. It is a member of the Canes Venatici I Group of galaxies [Kaisin & Karachentsev \(2008\)](#) and is at a distance of about 5.8 Mpc. It is also known as Mrk 209, I Zw 36, UGCA 281 and PGC 40665. The H I scale height of this galaxy is 220 pc and the H I disk radius is ≈ 2.3 kpc respectively. The galaxy has two intact holes.

A.26. *Haro 36*

Haro 36 (PGC 43124, UGC 7950) is located about 9.3 Mpc away and is the second most distant galaxy in the sample. It is a galaxy with a kiloparsec-sized Type 3 hole with expansion velocity 18 km s^{-1} . Interestingly, the size of this intact hole is larger than the galaxy's scale height of 220 pc, which suggests that the hole might not be completely spherical in nature. The rotational velocity of the galaxy is $\approx 76 \text{ km s}^{-1}$.

A.27. *IC 10*

IC 10, PGC 1305, or UGC 192 is a well-studied Local Group blue compact dwarf galaxy. It is located in the constellation Cassiopeia, at a distance of 0.7 Mpc, with V-band magnitude -16.3 . [Wilcots & Miller \(1998\)](#) first studied the holes in IC 10 and found eight holes. Based on our criteria, we detected 20 holes, most of which are Type 1. Our analysis shows that the large holes discovered by [Wilcots & Miller \(1998\)](#) contain two or more smaller holes and some of them are overlapped. We estimated the scale height of the galaxy as 190 pc.

A.28. *IC 1613*

IC 1613 (PGC 3844, UGC 668, DDO 8) is also a Local Group dwarf. It lies in the constellation of Cetus at a distance of 0.7 Mpc. [Lozinskaya et al. \(2003\)](#) found three large H I shells with expansion velocities of 15 to 18 km s⁻¹. [Silitch et al. \(2006\)](#) recalculated the expansion velocities for those regions to be 10 to 20 km s⁻¹. In our data, since all 11 holes we detected were Type 1, we used the velocity dispersion (6 km s⁻¹) of the quiescent regions of the galaxy as the expansion rate of the holes. The estimated scale height of this galaxy is 220 pc.

A.29. *LGS 3*

LGS 3, also known as the Pisces Dwarf or PGC 3792, is one of the smallest members of the Local Group, lies about 0.7 Mpc away, and is suspected to be a satellite of the Triangulum galaxy. Among the LITTLE THINGS galaxies, it has the smallest H I disk radius of (0.4 kpc), and smallest scale height of (60 pc). The velocity dispersion of the gas is also the lowest (≈ 5 km s⁻¹) in the sample. The galaxy has seven quite small holes including the smallest hole (27 pc) in our catalog.

A.30. *M81dwA*

M81dwA (PGC 23521) is one of the extremely faint (V-band magnitude ≈ -11.7) dwarfs in the M81 group, and is about a distance of 3.5 Mpc. The inner part of the H I disk of the galaxy is almost covered by a giant kiloparsec-sized Type 1 hole. The galaxy also contains one Type 2 and eight Type 3 holes in the outer part of the disk.

A.31. *Mrk 178*

Mrk 178 (UGC 6541, PGC 35684) is a BCD located 3.9 Mpc away from the Milky Way in the Canes Venatici I Group, and has a V-band magnitude of -14.1 . The H I structure of the galaxy was studied by [Stil & Israel \(2002\)](#) but they didn't report on any notable H I structures. We detected a large Type 2 hole expanding with ≈ 16 km s⁻¹ in the inner part of the disk.

A.32. *NGC 1569*

NGC 1569 (UGC 3056, VIIZw 16 or Arp 210) has less total H I gas in comparison to other dwarfs, has recently experienced a starburst, and has hot gas outflows. Therefore, it might be transitioning from a dwarf irregular to a dwarf elliptical galaxy ([Dellenbusch et al. 2008](#); [Angeretti et al. 2005](#); [Larsen et al. 2008](#); [Hunter & Elmegreen 2006](#)). The galaxy is about 3.4 Mpc away in the IC 342 (Maffei 1) Group and in the constellation Camelopardalis. We estimated the scale height of the galaxy to be ≈ 220 pc. The galaxy has five holes, with the highest expansion velocities in our sample, ranging from 22 to 30 km s⁻¹.

A.33. *NGC 2366*

NGC 2366, PGC 21102, UGC 3851, or DDO 42 is an M81 Group member located in the constellation Camelopardalis, and is at a distance of 3.4 Mpc. We detected 11 H I holes in the ISM of the galaxy. In the northern part of the H I disk, there appears to be a large Type 1 hole, but it is just a region where the flux density is below the threshold. The estimated scale height of the galaxy is about 400 pc.

A.34. *NGC 3738*

NGC 3738 (UGC 6565, Arp 234) is located at a distance of 1 Mpc in the Canes Venatici I Group and oriented face-on to us. It has a V-band magnitude of -17.1 . It contains three small completely broken holes.

A.35. *NGC 4163*

NGC 4163, also known as UGC 7199 and PGC 38881, is located at a distance of about 2.9 Mpc. According to our selection criteria, we couldn't detect any hole in this galaxy. We estimated the scale height of the galaxy to be about 140 pc and the H I disk length as 800 pc.

A.36. *NGC 4214*

NGC 4214 (UGC 7278, PGC 39225) is a Magellanic starburst dwarf located at a distance of 3 Mpc [de Vaucouleurs et al. \(1991\)](#) in the M94 Group. We credited only 21 holes out of 55 initially detected structures, which is less than half of the 56 holes found by [Bagetakos et al. \(2011\)](#). Among them about 71% are Type 1 holes. The galaxy also contains four holes larger than a kiloparsec, including the largest hole (≈ 2.3 kpc) detected in the LITTLE THINGS sample. The galaxy also has the highest rotational velocity (77 km s^{-1}) among all. The estimated H I scale height and H I disk radius of the galaxy are about 300 pc and 6.3 kpc respectively.

A.37. *SagDIG*

The Sagittarius dwarf irregular galaxy (SagDIG), also known as Lowal’s Object or PGC 63287, is an isolated satellite of the Milky Way about 1.1 Mpc away. The H I disk of SagDIG is dominated by a large Type 1 Hole of diameter ≈ 666 pc. The scale height of the galaxy is about 650 pc which is the highest in LITTLE THINGS sample according to our estimate.

A.38. *UGC 8508*

UGC 8508 (PGC 47495, IZw 60) is 2.6 Mpc away from the Milky Way in the M101 Group with V-band magnitude -13.6 . The galaxy has a large Type 1 hole near its center and two intact holes are in the periphery of the H I disk. The estimated H I scale height and the H I disk radius of the galaxy are ≈ 140 pc and ≈ 1.4 kpc respectively.

A.39. *WLM*

Wolf-Lundmark-Melott (WLM), also known as UGCA 444 or DDO 221, is an isolated dwarf which lies at the outer edges of the Local Group. It is located about a distance of 1 Mpc from the Milky Way with a V-band magnitude of -14.4 . All four holes of this galaxy are Type 1. The absence of Type 2 and Type 3 holes might be due to its small H I scale height, which is only about 100 pc.

A.40. *VIIZw 403*

VIIZw 403, also known as UGC 6456 and PGC 5286, is an isolated dwarf at a distance of about 4.4 Mpc, and is considered as a member of the M81 Group. [Simpson et al. \(2011\)](#) found an H I cavity coincident with the center of the H I velocity field but our criteria didn’t define that cavity as a hole. We didn’t detect any holes in this galaxy according to our selection criteria.

B. HOLE PROPERTIES OF LITTLE THINGS GALAXIES

Table 4. Hole Properties of CVnldwA

Hole No.	RA (J2000) (h m s)	Dec (J2000) (d m s)	v_{hel} (km s ⁻¹)	v_{exp} (km s ⁻¹)	Hole Type	PA (deg)	d (pc)	Age (Myr)	$\log n_{\text{H I}}$ ($\times 10^{20} \text{ cm}^{-2}$)	R (kpc)	Axial Ratio	H I mass $\times 10^4 M_{\odot}$	$\log E_{\text{Mc}}$ $\times 10^{50} \text{ (ergs)}$	$\log E_{\text{Ch}}$ $\times 10^{50} \text{ (ergs)}$
1	12 38 40.5	32 45 34.0	308	8	1	45	248	15.2	1.1	0.8	0.7	4	0.72	0.95

Table 5. Hole Properties of DDO 43

Hole No.	RA (J2000) (h m s)	Dec (J2000) (d m s)	v_{hel} (km s ⁻¹)	v_{exp} (km s ⁻¹)	Hole Type	PA (deg)	d (pc)	Age (Myr)	$\log N_{\text{HI}}$ ($\times 10^{20} \text{ cm}^{-2}$)	R (kpc)	Axial Ratio	H I mass $\times 10^4 M_{\odot}$	$\log E_{\text{Mc}}$ $\times 10^{50} \text{ (ergs)}$	$\log E_{\text{Ch}}$ $\times 10^{50} \text{ (ergs)}$
1	07 28 11.6	40 46 0.5	375	10	3	90	794	38.8	0.4	3.9	1.0	29	1.73	1.62
2	07 28 12.4	40 46 37.4	377	13	2	90	567	21.3	0.4	3.7	1.0	12	1.49	1.72
3	07 28 12.9	40 46 25.5	377	11	2	39	553	24.6	0.6	3.2	0.5	14	1.48	1.59
4	07 28 14.5	40 46 37.5	388	16	2	90	454	13.9	0.8	2.4	1.0	13	1.66	2.10
5	07 28 15.4	40 45 54.0	351	13	2	90	454	17.1	0.8	1.6	1.0	15	1.60	1.90
6	07 28 15.8	40 47 15.0	364	8	3	90	477	29.1	0.7	2.8	1.0	12	1.20	1.15
7	07 28 16.4	40 46 45.0	364	8	3	90	454	27.7	0.9	1.6	1.0	18	1.40	1.34
8	07 28 16.8	40 46 37.5	370	10	2	131	452	22.1	0.9	1.2	0.8	18	1.56	1.65
9	07 28 17.4	40 45 55.5	354	8	1	171	797	48.7	0.8	0.7	0.6	84	2.11	1.78
10	07 28 19.1	40 45 7.5	346	8	3	90	749	45.8	0.6	2.7	1.0	36	1.70	1.44
11	07 28 19.8	40 45 57.0	333	9	3	90	386	21.0	0.8	1.5	1.0	9	1.15	1.25
12	07 28 19.8	40 46 48.0	357	8	2	90	613	37.5	0.8	1.8	1.0	31	1.64	1.46
13	07 28 20.6	40 45 46.5	349	10	2	90	636	31.1	0.7	2.2	1.0	32	1.79	1.75
14	07 28 22.7	40 45 55.4	343	8	2	138	462	28.2	0.6	3.3	0.8	9	1.08	1.05
15	07 28 22.8	40 46 17.9	349	7	3	90	499	34.9	0.6	3.3	1.0	11	1.11	0.94

Table 6. Hole Properties of DDO 46

Hole No.	RA (J2000) (h m s)	Dec (J2000) (d m s)	v_{hel} (km s ⁻¹)	v_{exp} (km s ⁻¹)	Hole Type	PA (deg)	d (pc)	Age (Myr)	$\log N_{\text{HI}}$ ($\times 10^{20} \text{ cm}^{-2}$)	R (kpc)	Axial Ratio	H I mass $\times 10^4 M_{\odot}$	$\log E_{\text{Mc}}$ $\times 10^{50} \text{ (ergs)}$	$\log E_{\text{Ch}}$ $\times 10^{50} \text{ (ergs)}$
1	07 41 18.4	40 06 7.9	384	7	3	90	320	22.3	0.8	2.9	1.0	76	1.46	1.41
2	07 41 20.5	40 06 22.9	381	15	2	27	413	13.4	0.9	2.1	0.6	141	2.32	2.67
3	07 41 20.6	40 06 56.8	389	8	3	90	355	21.7	0.8	2.1	1.0	92	1.67	1.67
4	07 41 21.1	40 06 0.4	395	10	2	6	435	21.3	1.0	2.2	0.7	233	2.34	2.36
5	07 41 21.6	40 06 34.9	397	13	2	163	391	14.7	0.9	1.7	0.7	133	2.18	2.46
6	07 41 21.6	40 07 15.4	384	8	3	35	217	13.3	0.7	2.1	0.7	5	0.89	1.13
7	07 41 22.6	40 06 56.0	379	15	2	25	312	10.2	1.0	1.5	0.6	111	2.08	2.57
8	07 41 24.5	40 07 6.5	380	9	1	90	621	33.8	1.0	1.2	1.0	388	2.65	2.45
9	07 41 25.4	40 06 20.0	374	9	1	34	743	40.3	1.1	0.7	0.7	754	3.04	2.73
10	07 41 25.6	40 05 39.5	363	10	3	136	510	24.9	0.9	2.0	0.8	221	2.36	2.34
11	07 41 26.1	40 06 38.0	369	8	3	174	264	16.1	1.0	0.2	0.8	19	1.49	1.60
12	07 41 26.1	40 05 24.5	361	7	3	90	391	27.3	0.8	2.5	1.0	108	1.71	1.56
13	07 41 26.6	40 07 0.5	371	8	3	90	302	18.4	1.2	0.7	1.0	148	1.84	1.87
14	07 41 27.0	40 06 42.5	370	10	3	100	353	17.3	1.1	0.2	0.8	188	2.15	2.27
15	07 41 28.2	40 05 26.0	353	6	3	90	462	37.6	0.8	2.5	1.0	144	1.81	1.49
16	07 41 28.2	40 07 11.0	358	10	3	90	426	20.8	1.1	1.2	1.0	264	2.38	2.42
17	07 41 28.6	40 06 21.5	348	15	2	49	330	10.7	1.0	0.9	0.7	132	2.20	2.64
18	07 41 29.4	40 06 53.0	338	9	1	169	439	23.9	1.0	1.1	0.5	224	2.26	2.21

Table 7. Hole Properties of DDO 47

Hole No.	RA (J2000) (h m s)	Dec (J2000) (d m s)	v_{hel} (km s ⁻¹)	v_{exp} (km s ⁻¹)	Hole Type	PA (deg)	d (pc)	Age (Myr)	$\log N_{\text{HI}}$ ($\times 10^{20} \text{cm}^{-2}$)	R (kpc)	Axial Ratio	H I mass $\times 10^4 M_{\odot}$	$\log E_{\text{Mc}}$ $\times 10^{50} (\text{ergs})$	$\log E_{\text{Ch}}$ $\times 10^{50} (\text{ergs})$
1	07 41 46.7	16 47 32.3	288	9	1	89	1100	59.7	0.7	5.1	0.7	79	2.11	1.77
2	07 41 46.9	16 49 27.8	301	9	1	60	829	45.0	0.7	4.0	0.3	35	1.75	1.53
3	07 41 49.5	16 47 12.8	280	9	1	105	428	23.3	0.7	4.9	0.8	4	0.80	0.92
4	07 41 49.9	16 46 32.3	270	9	1	90	1211	65.8	0.6	6.8	1.0	93	2.18	1.79
5	07 41 50.7	16 48 41.3	290	15	2	162	668	21.8	0.8	1.9	0.5	20	1.81	2.06
6	07 41 52.3	16 47 36.8	281	11	2	90	454	20.2	0.9	2.6	1.0	9	1.26	1.45
7	07 41 53.4	16 46 47.3	268	8	3	90	484	29.6	0.7	5.0	1.0	8	0.98	0.95
8	07 41 54.2	16 48 35.3	283	9	1	145	769	41.8	0.8	1.3	0.7	36	1.77	1.58
9	07 41 54.2	16 47 29.3	268	9	3	90	409	22.2	0.9	2.4	1.0	6	0.98	1.09
10	07 41 54.7	16 49 28.0	286	8	3	90	457	27.9	0.8	4.3	0.6	8	0.99	0.97
11	07 41 55.7	16 50 23.3	291	9	1	101	837	45.5	0.7	7.6	0.7	35	1.74	1.53
12	07 41 56.1	16 49 54.8	286	9	1	87	439	23.8	0.8	6.1	0.7	6	0.93	1.03
13	07 41 57.7	16 48 35.3	265	9	1	90	681	37.0	0.8	2.3	1.0	25	1.60	1.47
14	07 41 58.2	16 47 56.3	265	8	3	90	530	32.4	0.7	1.1	1.0	10	1.08	1.02
15	07 41 58.8	16 47 15.8	257	9	1	37	1623	88.2	0.8	2.5	0.9	869	2.74	2.19
16	07 42 0.1	16 48 37.3	268	13	2	65	524	19.7	0.9	3.3	0.8	12	1.51	1.76
17	07 42 0.1	16 49 26.3	277	10	2	20	371	18.1	0.8	5.8	0.7	4	0.83	1.07
18	07 42 2.9	16 46 41.9	250	15	2	62	586	19.1	0.8	4.2	0.6	14	1.66	1.96
19	07 42 3.8	16 48 12.7	255	9	1	61	927	50.3	0.7	4.0	0.7	51	1.92	1.65

Table 8. Hole Properties of DDO 50

Hole No.	RA (J2000) (h m s)	Dec (J2000) (d m s)	v_{hel} (km s ⁻¹)	v_{exp} (km s ⁻¹)	Hole Type	PA (deg)	d (pc)	Age (Myr)	$\log N_{\text{H I}}$ ($\times 10^{20} \text{ cm}^{-2}$)	R (kpc)	Axial Ratio	H I mass $\times 10^4 M_{\odot}$	$\log E_{\text{Mc}}$ $\times 10^{50} \text{ (ergs)}$	$\log E_{\text{Ch}}$ $\times 10^{50} \text{ (ergs)}$
1	08 18 22.2	70 44 29.1	152	9	1	110	1521	82.6	0.7	5.7	0.5	971	2.75	2.22
2	08 18 28.0	70 42 18.7	168	9	1	17	990	53.8	1.0	4.6	0.6	161	2.48	2.12
3	08 18 31.5	70 45 36.8	142	9	1	174	961	52.2	0.6	5.3	0.4	67	2.04	1.76
4	08 18 36.0	70 44 42.1	153	18	3	90	742	20.2	0.9	4.3	1.0	66	2.49	2.76
5	08 18 38.2	70 46 44.4	137	9	1	136	1011	54.9	0.6	5.5	0.8	81	2.15	1.81
6	08 18 38.8	70 45 47.4	147	9	1	73	926	50.3	0.6	4.7	0.6	57	1.97	1.70
7	08 18 39.9	70 41 36.9	163	9	1	90	792	43.0	0.8	3.4	1.0	59	2.00	1.78
8	08 18 42.6	70 40 54.9	163	15	1	180	203	6.6	0.9	3.5	0.5	1	0.59	1.37
9	08 18 49.2	70 43 40.0	147	9	1	42	348	18.9	0.9	2.3	0.8	6	0.94	1.11
10	08 18 52.8	70 42 47.5	163	10	3	90	198	9.7	1.2	1.8	1.0	3	0.67	1.15
11	08 18 54.4	70 41 28.1	168	9	1	20	653	35.5	0.8	2.3	0.9	33	1.74	1.61
12	08 18 55.3	70 38 52.1	178	9	1	35	1192	64.7	0.8	4.6	0.7	210	2.58	2.16
13	08 18 57.5	70 42 58.1	163	12	3	90	594	24.2	1.2	1.3	1.0	61	2.23	2.30
14	08 18 58.2	70 45 37.1	137	9	1	87	848	46.1	0.9	2.8	0.7	87	2.18	1.92
15	08 18 59.5	70 44 58.1	132	9	1	43	585	31.8	1.0	2.1	0.7	33	1.76	1.66
16	08 19 2.8	70 43 32.6	158	9	1	90	693	37.6	1.0	0.7	1.0	61	2.04	1.86
17	08 19 5.8	70 45 59.6	137	9	1	83	275	14.9	0.7	2.8	0.6	2	0.49	0.79
18	08 19 5.9	70 41 23.6	178	9	1	47	1889	102.6	1.1	2.1	0.7	3541	3.46	2.78
19	08 19 7.6	70 46 4.1	131	10	2	85	330	16.1	0.8	2.8	0.8	5	0.91	1.19
20	08 19 7.6	70 45 43.1	137	11	2	60	293	13.0	0.9	2.4	0.7	4	0.86	1.25
21	08 19 9.5	70 46 16.1	147	15	2	135	388	12.6	0.9	3.0	0.7	9	1.48	1.94
22	08 19 12.8	70 44 29.6	147	9	1	15	840	45.6	0.9	1.1	0.9	90	2.20	1.94
23	08 19 13.1	70 45 25.1	142	11	2	45	469	20.9	1.0	2.0	0.9	20	1.64	1.79
24	08 19 17.1	70 46 52.1	142	9	1	90	297	16.1	0.8	3.5	1.0	3	0.71	0.96
25	08 19 19.2	70 45 31.1	132	15	2	93	181	5.9	1.0	2.3	0.4	1	0.54	1.37
26	08 19 20.4	70 48 17.6	137	9	1	98	495	26.9	0.6	5.0	1.0	9	1.15	1.19
27	08 19 23.1	70 48 8.6	137	9	1	122	602	32.7	0.7	4.8	0.9	21	1.54	1.46
28	08 19 23.4	70 43 28.1	153	9	1	39	709	38.5	0.9	1.7	0.6	57	2.00	1.81
29	08 19 25.2	70 42 19.1	183	15	2	90	376	12.3	1.2	2.4	1.0	15	1.73	2.18
30	08 19 25.6	70 45 26.6	147	8	3	90	346	21.2	0.9	2.5	1.0	6	0.91	1.00
31	08 19 26.2	70 45 28.1	142	10	3	90	346	16.9	0.9	2.6	1.0	6	1.04	1.29
32	08 19 27.8	70 41 06.8	173	10	3	90	495	24.2	1.0	3.6	1.0	23	1.65	1.71
33	08 19 28.0	70 45 25.1	147	8	3	90	495	30.2	0.9	2.7	1.0	19	1.45	1.35
34	08 19 28.8	70 39 49.1	173	9	1	90	742	40.3	0.8	4.8	1.0	50	1.93	1.74
35	08 19 29.2	70 43 35.6	153	9	1	54	359	19.5	0.9	2.3	0.8	7	1.04	1.19
36	08 19 33.1	70 45 14.6	153	9	1	118	505	27.4	0.9	3.0	0.6	17	1.43	1.43
37	08 19 35.4	70 41 27.3	168	15	3	90	544	17.7	1.1	4.1	1.0	35	2.11	2.39
38	08 19 37.4	70 45 1.1	158	9	1	108	325	17.7	0.9	3.4	0.5	5	0.88	1.07
39	08 19 37.8	70 43 12.3	153	10	2	90	594	29.0	1.1	3.4	1.0	45	1.97	1.93
40	08 19 40.7	70 46 14.6	147	9	1	133	1784	96.9	0.8	4.2	0.5	1875	3.11	2.51
41	08 19 45.2	70 42 49.0	163	11	2	88	434	19.3	0.8	4.4	0.6	10	1.34	1.54

Table 9. Hole Properties of DDO 52

Hole No.	RA (J2000) (h m s)	Dec (J2000) (d m s)	v_{hel} (km s ⁻¹)	v_{exp} (km s ⁻¹)	Hole Type	PA (deg)	d (pc)	Age (Myr)	$\log N_{\text{HI}}$ ($\times 10^{20} \text{ cm}^{-2}$)	R (kpc)	Axial Ratio	H I mass $\times 10^4 M_{\odot}$	$\log E_{\text{Mc}}$ $\times 10^{50} \text{ (ergs)}$	$\log E_{\text{Ch}}$ $\times 10^{50} \text{ (ergs)}$
1	08 28 23.7	41 51 46.4	413	11	2	90	599	26.6	0.5	4.5	1.0	98	1.88	1.92
2	08 28 25.7	41 50 49.5	376	10	2	173	487	23.8	0.7	2.8	0.5	84	1.67	1.73
3	08 28 26.2	41 51 37.5	407	10	3	15	734	35.9	0.7	2.2	0.7	219	2.28	2.14
4	08 28 26.6	41 51 3.5	389	10	2	179	804	39.3	0.7	1.8	0.5	269	2.43	2.23
5	08 28 26.7	41 49 42.0	363	10	2	40	464	22.7	0.4	5.1	0.6	10	1.28	1.40
6	08 28 26.9	41 52 45.0	438	8	1	15	382	23.3	0.4	4.6	0.5	6	0.90	0.96
7	08 28 27.4	41 52 34.5	428	12	3	90	599	24.4	0.6	3.9	1.0	106	1.97	2.06
8	08 28 28.1	41 51 51.0	415	13	2	24	821	30.9	0.6	1.6	0.8	219	2.49	2.48
9	08 28 28.5	41 49 55.5	358	8	1	11	413	25.3	0.6	4.3	0.5	11	1.20	1.20
10	08 28 28.5	41 52 12.0	425	10	3	90	480	23.5	0.5	2.6	1.0	61	1.51	1.58
11	08 28 28.5	41 50 37.5	376	15	2	137	596	19.4	0.8	2.2	0.8	184	2.38	2.59
12	08 28 29.4	41 52 12.0	423	8	1	42	518	31.7	0.3	2.6	0.6	46	1.26	1.18
13	08 28 30.1	41 51 37.5	415	13	3	70	526	19.8	0.8	1.6	0.6	129	2.08	2.25
14	08 28 30.9	41 51 4.5	384	8	1	58	523	31.9	0.7	2.4	0.8	114	1.71	1.57
15	08 28 32.1	41 51 45.8	410	8	1	69	634	38.8	0.6	3.4	0.6	135	1.86	1.64
16	08 28 33.0	41 51 16.4	410	15	3	90	959	31.3	0.5	4.1	1.0	243	2.69	2.71
17	08 28 34.7	41 52 31.4	431	12	3	90	569	23.2	0.3	6.3	1.0	53	1.61	1.76

Table 10. Hole Properties of DDO 53

Hole No.	RA (J2000) (h m s)	Dec (J2000) (d m s)	v_{hel} (km s ⁻¹)	v_{exp} (km s ⁻¹)	Hole Type	PA (deg)	d (pc)	Age (Myr)	$\log N_{\text{H I}}$ ($\times 10^{20} \text{ cm}^{-2}$)	R (kpc)	Axial Ratio	H I mass $\times 10^4 M_{\odot}$	$\log E_{\text{Mc}}$ $\times 10^{50} \text{ (ergs)}$	$\log E_{\text{Ch}}$ $\times 10^{50} \text{ (ergs)}$
1	08 34 3.5	66 11 6.4	7	15	3	90	272	8.9	1.0	1.4	1.0	3	1.00	1.64
2	08 34 3.8	66 10 21.5	23	8	3	90	210	12.8	1.1	0.7	1.0	2	0.34	0.66
3	08 34 4.8	66 10 39.5	7	10	3	90	126	6.1	1.1	0.4	1.0	0	-0.17	0.55
4	08 34 5.3	66 10 30.5	17	8	3	30	170	10.4	1.1	0.3	0.5	1	0.08	0.48
5	08 34 7.5	66 11 41.0	23	8	3	10	255	15.6	0.7	2.6	0.5	1	0.18	0.45
6	08 34 10.0	66 10 38.0	23	9	1	16	339	18.4	1.1	0.2	0.9	8	1.11	1.27
7	08 34 11.4	66 11 21.5	15	11	3	90	293	13.0	1.0	1.7	1.0	4	0.93	1.32

Table 11. Hole Properties of DDO 63

Hole No.	RA (J2000) (h m s)	Dec (J2000) (d m s)	v_{hel} (km s ⁻¹)	v_{exp} (km s ⁻¹)	Hole Type	PA (deg)	d (pc)	Age (Myr)	$\log N_{\text{H I}}$ ($\times 10^{20} \text{ cm}^{-2}$)	R (kpc)	Axial Ratio	H I mass $\times 10^4 M_{\odot}$	$\log E_{\text{Mc}}$ $\times 10^{50} \text{ (ergs)}$	$\log E_{\text{Ch}}$ $\times 10^{50} \text{ (ergs)}$
1	09 40 13.9	71 11 30.6	146	8	3	90	431	26.4	0.9	1.6	1.0			
2	09 40 22.1	71 12 21.5	144	10	3	90	250	12.2	0.9	1.7	1.0			
3	09 40 22.4	71 12 8.0	149	15	2	178	208	6.8	1.0	1.4	0.6			
4	09 40 22.7	71 12 33.5	136	8	1	147	323	19.7	0.9	1.9	0.9			
5	09 40 28.6	71 12 10.7	136	11	3	90	318	14.1	0.9	1.3	1.0			
6	09 40 30.6	71 11 9.2	141	8	1	102	950	58.0	1.0	0.1	0.7			
7	09 40 35.2	71 09 59.9	154	15	2	160	282	9.2	1.1	1.3	0.8			

Table 12. Hole Properties of DDO 69

Hole No.	RA (J2000) (h m s)	Dec (J2000) (d m s)	v_{hel} (km s ⁻¹)	v_{exp} (km s ⁻¹)	Hole Type	PA (deg)	d (pc)	Age (Myr)	$\log N_{\text{H I}}$ ($\times 10^{20} \text{ cm}^{-2}$)	R (kpc)	Axial Ratio	H I mass $\times 10^4 M_{\odot}$	$\log E_{\text{Mc}}$ $\times 10^{50} \text{ (ergs)}$	$\log E_{\text{Ch}}$ $\times 10^{50} \text{ (ergs)}$
1	09 59 13.8	30 44 19.8	27	7	1	137	56	3.9	0.7	0.6	0.6	0	-1.57	-0.70
2	09 59 21.0	30 44 36.3	26	7	1	14	331	23.1	0.9	0.2	0.4	11	1.11	1.08
3	09 59 26.6	30 44 25.8	28	12	2	38	38	1.5	0.9	0.2	0.5	0	-1.52	-0.12
4	09 59 30.2	30 44 9.3	25	10	2	5	77	3.8	1.0	0.5	0.4	0	-0.52	0.40

Table 13. Hole Properties of DDO 70

Hole No.	RA (J2000) (h m s)	Dec (J2000) (d m s)	v_{hel} (km s ⁻¹)	v_{exp} (km s ⁻¹)	Hole Type	PA (deg)	d (pc)	Age (Myr)	$\log N_{\text{H I}}$ ($\times 10^{20} \text{ cm}^{-2}$)	R (kpc)	Axial Ratio	H I mass $\times 10^4 M_{\odot}$	$\log E_{\text{Mc}}$ $\times 10^{50} \text{ (ergs)}$	$\log E_{\text{Ch}}$ $\times 10^{50} \text{ (ergs)}$
1	09 59 47.6	05 19 41.4	289	9	1	12	246	13.4	0.5	1.2	0.5	2	0.36	0.70
2	09 59 53.5	05 22 1.0	304	9	1	116	723	39.3	0.7	1.7	0.8	177	2.04	1.84
3	09 59 53.5	05 20 20.5	296	9	1	178	347	18.8	0.8	0.8	0.4	9	1.18	1.32
4	09 59 57.2	05 17 28.0	293	9	1	87	791	43.0	0.7	1.7	0.8	221	2.18	1.94
5	09 59 57.7	05 18 38.5	291	13	2	90	235	8.8	0.8	0.9	1.0	3	0.89	1.48
6	09 59 59.4	05 19 32.5	296	9	1	137	171	9.3	1.0	0.2	0.7	2	0.38	0.86
7	10 00 2.8	05 19 41.5	299	9	1	93	251	13.6	0.9	0.2	0.7	4	0.82	1.11
8	10 00 5.0	05 18 38.5	302	9	1	160	321	17.4	0.9	0.9	0.8	8	1.11	1.29
9	10 00 7.3	05 20 5.5	311	9	1	90	303	16.4	0.8	0.6	1.0	6	0.98	1.19

Table 14. Hole Properties of DDO 75

Hole No.	RA (J2000) (h m s)	Dec (J2000) (d m s)	v_{hel} (km s ⁻¹)	v_{exp} (km s ⁻¹)	Hole Type	PA (deg)	d (pc)	Age (Myr)	$\log N_{\text{H I}}$ ($\times 10^{20} \text{ cm}^{-2}$)	R (kpc)	Axial Ratio	H I mass $\times 10^4 M_{\odot}$	$\log E_{\text{Mc}}$ $\times 10^{50} (\text{ergs})$	$\log E_{\text{Ch}}$ $\times 10^{50} (\text{ergs})$
1	10 10 55.3	-04 42 31.0	316	9	1	152	269	14.6	0.9	0.4	0.6	7	1.08	1.32
2	10 11 6.1	-04 41 26.5	336	9	1	90	303	16.4	1.2	0.7	1.0	19	1.56	1.71
3	10 11 1.1	-04 41 7.0	316	9	1	123	1195	64.9	1.0	0.4	0.6	1428	3.18	2.68
4	10 11 2.2	-04 43 41.5	316	9	1	114	312	17.0	0.9	0.8	0.6	11	1.28	1.44

Table 15. Hole Properties of DDO 87

Hole No.	RA (J2000) (h m s)	Dec (J2000) (d m s)	v_{hel} (km s ⁻¹)	v_{exp} (km s ⁻¹)	Hole Type	PA (deg)	d (pc)	Age (Myr)	$\log N_{\text{H I}}$ ($\times 10^{20} \text{ cm}^{-2}$)	R (kpc)	Axial Ratio	H I mass $\times 10^4 M_{\odot}$	$\log E_{\text{Mc}}$ $\times 10^{50} (\text{ergs})$	$\log E_{\text{Ch}}$ $\times 10^{50} (\text{ergs})$
1	10 49 21.0	65 30 43.9	374	8	3	90	515	31.5	0.5	4.6	1.0	9	1.08	1.01
2	10 49 21.7	65 31 33.4	364	7	1	90	1344	93.9	0.5	3.1	1.0	382	2.26	1.63
3	10 49 25.1	65 30 57.4	364	7	1	90	1344	93.9	0.6	3.5	1.0	467	2.34	1.72
4	10 49 26.5	65 32 1.9	361	11	2	172	491	21.8	0.7	2.6	0.5	12	1.40	1.55
5	10 49 28.7	65 32 39.4	343	7	1	180	1820	127.2	0.5	4.4	0.5	762	2.71	1.93
6	10 49 31.6	65 33 18.5	320	10	2	43	475	23.2	0.5	6.8	0.7	6	1.04	1.17
7	10 49 32.1	65 31 56.0	351	10	2	5	691	33.8	0.8	1.1	0.8	36	1.84	1.76
8	10 49 32.9	65 31 4.8	354	8	3	90	851	52.0	0.6	2.8	1.0	51	1.85	1.53
9	10 49 33.3	65 31 48.5	338	9	3	90	762	41.4	0.7	0.4	1.0	42	1.85	1.66
10	10 49 36.0	65 30 44.1	355	15	2	140	693	22.6	0.7	4.5	0.9	33	2.04	2.26
11	10 49 36.2	65 29 59.0	356	8	2	177	356	21.7	0.4	7.6	0.8	2	0.38	0.51
12	10 49 37.6	65 31 42.5	330	10	3	90	403	19.7	0.7	0.8	1.0	6	1.04	1.25
13	10 49 38.8	65 32 31.9	325	7	1	89	1406	98.2	0.6	3.1	0.6	510	2.41	1.76
14	10 49 40.0	65 31 31.4	341	10	3	90	672	32.9	0.6	1.9	1.0	25	1.68	1.62
15	10 49 41.0	65 30 43.9	338	7	1	178	671	46.9	0.5	5.1	0.9	19	1.32	1.05
16	10 49 49.4	65 32 22.9	297	13	2	85	1098	41.3	0.4	3.8	0.7	204	2.26	2.16
17	10 49 51.6	65 31 10.9	328	11	2	39	480	21.3	0.4	5.5	0.6	5	1.00	1.22
18	10 49 55.0	65 32 16.9	304	6	3	90	627	51.1	0.3	4.9	1.0	10	0.91	0.58

Table 16. Hole Properties of DDO 101

Hole No.	RA (J2000) (h m s)	Dec (J2000) (d m s)	v_{hel} (km s ⁻¹)	v_{exp} (km s ⁻¹)	Hole Type	PA (deg)	d (pc)	Age (Myr)	$\log N_{\text{HI}}$ ($\times 10^{20} \text{ cm}^{-2}$)	R (kpc)	Axial Ratio	H I mass $\times 10^4 M_{\odot}$	$\log E_{\text{Mc}}$ $\times 10^{50} \text{ (ergs)}$	$\log E_{\text{Ch}}$ $\times 10^{50} \text{ (ergs)}$
1	11 55 38.1	31 31 5.0	626	16	2	86	355	10.9	0.5	0.6	0.5	34	1.85	2.36
2	11 55 38.5	31 31 27.5	600	10	3	90	335	16.4	0.6	0.9	1.0	35	1.56	1.75

Table 17. Hole Properties of DDO 126

Hole No.	RA (J2000) (h m s)	Dec (J2000) (d m s)	v_{hel} (km s ⁻¹)	v_{exp} (km s ⁻¹)	Hole Type	PA (deg)	d (pc)	Age (Myr)	$\log N_{\text{HI}}$ ($\times 10^{20} \text{ cm}^{-2}$)	R (kpc)	Axial Ratio	H I mass $\times 10^4 M_{\odot}$	$\log E_{\text{Mc}}$ $\times 10^{50} \text{ (ergs)}$	$\log E_{\text{Ch}}$ $\times 10^{50} \text{ (ergs)}$
1	12 27 2.0	37 08 46.5	203	9	1	170	477	25.9	1.0	2.0	0.7	25	1.63	1.62
2	12 27 3.7	37 09 15.0	200	12	3	132	465	19.0	1.1	1.6	0.7	26	1.85	2.04
3	12 27 7.8	37 08 36.0	220	9	1	116	650	35.3	1.0	1.3	0.8	206	2.04	1.88
4	12 27 11.7	37 07 56.9	234	9	1	6	996	54.1	0.9	2.4	0.6	391	2.52	2.16

Table 18. Hole Properties of DDO 133

Hole No.	RA (J2000) (h m s)	Dec (J2000) (d m s)	v_{hel} (km s ⁻¹)	v_{exp} (km s ⁻¹)	Hole Type	PA (deg)	d (pc)	Age (Myr)	$\log N_{\text{H I}}$ ($\times 10^{20} \text{ cm}^{-2}$)	R (kpc)	Axial Ratio	H I mass $\times 10^4 M_{\odot}$	$\log E_{\text{Mc}}$ $\times 10^{50} \text{ (ergs)}$	$\log E_{\text{Ch}}$ $\times 10^{50} \text{ (ergs)}$
1	12 32 50.7	31 31 26.1	318	10	1	19	573	28.0	0.7	1.8	0.7	131	1.96	1.93
2	12 32 52.1	31 30 36.6	310	10	1	57	612	29.9	0.6	2.1	0.5	112	1.90	1.86
3	12 32 56.4	31 33 56.1	352	10	1	90	856	41.8	0.7	1.8	1.0	320	2.54	2.32
4	12 32 57.2	31 31 48.6	321	10	1	180	494	24.2	0.9	0.7	0.6	142	1.94	1.96
5	12 32 59.5	31 32 53.1	336	10	1	150	545	26.6	0.8	1.6	0.7	166	2.04	2.03

Table 19. Hole Properties of DDO 154

Hole No.	RA (J2000) (h m s)	Dec (J2000) (d m s)	v_{hel} (km s ⁻¹)	v_{exp} (km s ⁻¹)	Hole Type	PA (deg)	d (pc)	Age (Myr)	$\log N_{\text{H I}}$ ($\times 10^{20} \text{ cm}^{-2}$)	R (kpc)	Axial Ratio	H I mass $\times 10^4 M_{\odot}$	$\log E_{\text{Mc}}$ $\times 10^{50} (\text{ergs})$	$\log E_{\text{Ch}}$ $\times 10^{50} (\text{ergs})$
1	12 53 58.2	27 08 28.5	403	5	3	90	248	24.2	1.0	2.6	1.0	2	0.18	0.09
2	12 54 1.5	27 08 26.0	403	8	1	132	305	18.7	1.1	1.4	0.7	6	0.89	1.02
3	12 54 2.9	27 07 54.0	403	8	1	28	464	28.4	0.9	1.9	0.6	12	1.23	1.18
4	12 54 3.0	27 09 17.0	385	5	2	90	183	17.9	1.2	1.4	1.0	1	-0.07	-0.02
5	12 54 3.4	27 08 48.5	388	8	1	90	485	29.6	1.2	0.8	1.0	26	1.59	1.49
6	12 54 6.2	27 08 20.0	385	8	1	23	644	39.4	1.1	1.8	0.8	47	1.85	1.62
7	12 54 7.1	27 09 57.5	362	5	3	90	194	19.0	1.1	1.3	1.0	1	-0.06	-0.03
8	12 54 8.3	27 09 14.0	369	10	2	153	415	20.3	1.2	1.0	0.5	15	1.46	1.60
9	12 54 15.9	27 09 40.9	354	8	1	45	391	23.9	0.9	3.7	0.6	7	0.95	0.99

Table 20. Hole Properties of DDO 155

Hole No.	RA (J2000) (h m s)	Dec (J2000) (d m s)	v_{hel} (km s ⁻¹)	v_{exp} (km s ⁻¹)	Hole Type	PA (deg)	d (pc)	Age (Myr)	$\log N_{\text{H I}}$ ($\times 10^{20} \text{ cm}^{-2}$)	R (kpc)	Axial Ratio	H I mass $\times 10^4 M_{\odot}$	$\log E_{\text{Mc}}$ $\times 10^{50} \text{ (ergs)}$	$\log E_{\text{Ch}}$ $\times 10^{50} \text{ (ergs)}$
1	12 58 38.7	14 13 7.5	210	10	1	90	288	14.1	0.9	0.2	1.0	56	1.52	1.77
2	12 58 39.2	14 12 49.5	210	10	1	140	225	11.0	0.9	0.3	0.6	8	1.20	1.58
3	12 58 40.9	14 13 24.0	220	10	1	90	282	13.8	0.8	0.2	1.0	39	1.32	1.61

Table 21. Hole Properties of DDO 165

Hole No.	RA (J2000) (h m s)	Dec (J2000) (d m s)	v_{hel} (km s ⁻¹)	v_{exp} (km s ⁻¹)	Hole Type	PA (deg)	d (pc)	Age (Myr)	$\log N_{\text{H I}}$ ($\times 10^{20} \text{ cm}^{-2}$)	R (kpc)	Axial Ratio	H I mass $\times 10^4 M_{\odot}$	$\log E_{\text{Mc}}$ $\times 10^{50} \text{ (ergs)}$	$\log E_{\text{Ch}}$ $\times 10^{50} \text{ (ergs)}$
1	13 06 12.1	67 42 12.9	29	13	2	31	347	13.0	1.0	1.6	0.7	7	1.28	1.70
2	13 06 16.3	67 42 33.9	31	12	3	90	452	18.4	0.9	1.1	1.0	13	1.51	1.75
3	13 06 29.8	67 42 40.0	26	12	1	135	1797	73.2	0.7	0.8	0.7	1049	3.18	2.77

Table 22. Hole Properties of DDO 167

Hole No.	RA (J2000) (h m s)	Dec (J2000) (d m s)	v_{hel} (km s ⁻¹)	v_{exp} (km s ⁻¹)	Hole Type	PA (deg)	d (pc)	Age (Myr)	$\log N_{\text{HI}}$ ($\times 10^{20} \text{ cm}^{-2}$)	R (kpc)	Axial Ratio	H I mass $\times 10^4 M_{\odot}$	$\log E_{\text{Mc}}$ $\times 10^{50} \text{ (ergs)}$	$\log E_{\text{Ch}}$ $\times 10^{50} \text{ (ergs)}$
1	13 13 20.8	46 19 46.0	172	9	3	90	269	14.6	0.9	0.9	1.0	7	1.08	1.33
2	13 13 22.4	46 19 5.5	163	8	1	138	387	23.6	0.6	0.2	0.6	10	1.15	1.17
3	13 13 24.7	46 19 23.5	165	8	1	90	391	23.9	0.6	0.8	1.0	11	1.18	1.18

Table 23. Hole Properties of DDO 168

Hole No.	RA (J2000) (h m s)	Dec (J2000) (d m s)	v_{hel} (km s ⁻¹)	v_{exp} (km s ⁻¹)	Hole Type	PA (deg)	d (pc)	Age (Myr)	$\log N_{\text{HI}}$ ($\times 10^{20} \text{ cm}^{-2}$)	R (kpc)	Axial Ratio	H I mass $\times 10^4 M_{\odot}$	$\log E_{\text{Mc}}$ $\times 10^{50} \text{ (ergs)}$	$\log E_{\text{Ch}}$ $\times 10^{50} \text{ (ergs)}$
1	13 14 24.7	45 55 54.1	208	10	3	90	501	24.5	1.3	0.8	1.0	389	2.49	2.45
2	13 14 27.4	45 56 40.5	200	8	1	90	751	45.9	1.1	1.4	1.0	500	2.62	2.27

Table 24. Hole Properties of DDO 187

Hole No.	RA (J2000) (h m s)	Dec (J2000) (d m s)	v_{hel} (km s ⁻¹)	v_{exp} (km s ⁻¹)	Hole Type	PA (deg)	d (pc)	Age (Myr)	$\log N_{\text{H I}}$ ($\times 10^{20} \text{ cm}^{-2}$)	R (kpc)	Axial Ratio	H I mass $\times 10^4 M_{\odot}$	$\log E_{\text{Mc}}$ $\times 10^{50} \text{ (ergs)}$	$\log E_{\text{Ch}}$ $\times 10^{50} \text{ (ergs)}$
1	14 15 55.4	23 02 52.0	150	11	3	90	115	5.1	1.0	0.3	1.0	3	0.89	1.60
2	14 15 57.8	23 03 44.5	153	14	3	90	173	6.0	1.0	0.3	1.0	27	1.56	2.24
3	14 15 58.2	23 03 50.5	150	15	2	98	155	5.1	0.9	0.4	0.8	17	1.32	2.11

Table 25. Hole Properties of DDO 210

Hole No.	RA (J2000) (h m s)	Dec (J2000) (d m s)	v_{hel} (km s ⁻¹)	v_{exp} (km s ⁻¹)	Hole Type	PA (deg)	d (pc)	Age (Myr)	$\log N_{\text{HI}}$ ($\times 10^{20} \text{ cm}^{-2}$)	R (kpc)	Axial Ratio	H I mass $\times 10^4 M_{\odot}$	$\log E_{\text{Mc}}$ $\times 10^{50} \text{ (ergs)}$	$\log E_{\text{Ch}}$ $\times 10^{50} \text{ (ergs)}$
1	20 46 52.2	-12 51 9.6	-138	6	1	90	79	6.4	0.8	0.2	1.0	0	-0.82	-0.28

Table 26. Hole Properties of DDO 216

Hole No.	RA (J2000) (h m s)	Dec (J2000) (d m s)	v_{hel} (km s ⁻¹)	v_{exp} (km s ⁻¹)	Hole Type	PA (deg)	d (pc)	Age (Myr)	$\log N_{\text{H I}}$ ($\times 10^{20} \text{ cm}^{-2}$)	R (kpc)	Axial Ratio	H I mass $\times 10^4 M_{\odot}$	$\log E_{\text{Mc}}$ $\times 10^{50} \text{ (ergs)}$	$\log E_{\text{Ch}}$ $\times 10^{50} \text{ (ergs)}$
1	23 28 27.7	14 45 3.9	-193	9	3	90	147	8.0	0.5	0.7	1.0	1	-0.10	0.48
2	23 28 27.7	14 45 28.4	-189	8	3	90	320	19.6	0.6	0.6	1.0	17	0.94	1.05
3	23 28 33.6	14 45 56.4	-184	8	3	90	205	12.5	0.4	1.0	1.0	1	0.18	0.52

Table 27. Hole Properties of F564-V3

Hole No.	RA (J2000) (h m s)	Dec (J2000) (d m s)	v_{hel} (km s ⁻¹)	v_{exp} (km s ⁻¹)	Hole Type	PA (deg)	d (pc)	Age (Myr)	$\log N_{\text{H I}}$ ($\times 10^{20} \text{cm}^{-2}$)	R (kpc)	Axial Ratio	H I mass $\times 10^4 M_{\odot}$	$\log E_{\text{Mc}}$ $\times 10^{50} (\text{ergs})$	$\log E_{\text{Ch}}$ $\times 10^{50} (\text{ergs})$
1	09 02 51.0	20 04 17.0	489	11	3	90	835	37.1	0.3	2.1	1.0	139	2.45	2.30
2	09 02 51.2	20 04 30.5	487	9	3	90	962	52.3	0.4	1.9	1.0	232	2.62	2.27
3	09 02 52.7	20 03 35.0	464	9	2	140	588	32.0	0.0	2.4	0.6	37	1.54	1.47
4	09 02 53.0	20 05 0.5	493	8	3	168	680	41.6	0.3	1.5	0.5	99	2.00	1.74
5	09 02 53.6	20 04 9.5	486	15	2	62	650	21.2	0.5	0.8	0.6	135	2.52	2.70
6	09 02 54.2	20 03 54.5	460	10	2	145	877	42.9	0.2	1.5	0.8	125	2.34	2.14
7	09 02 54.4	20 03 41.0	468	8	3	122	702	42.9	0.0	2.1	0.8	49	1.67	1.44
8	09 02 54.5	20 04 59.0	491	9	3	1	1208	65.6	0.4	1.3	0.5	377	2.94	2.48

Table 28. Hole Properties of Haro 29

Hole No.	RA (J2000) (h m s)	Dec (J2000) (d m s)	v_{hel} (km s ⁻¹)	v_{exp} (km s ⁻¹)	Hole Type	PA (deg)	d (pc)	Age (Myr)	$\log N_{\text{HI}}$ ($\times 10^{20} \text{ cm}^{-2}$)	R (kpc)	Axial Ratio	H I mass $\times 10^4 M_{\odot}$	$\log E_{\text{Mc}}$ $\times 10^{50} \text{ (ergs)}$	$\log E_{\text{Ch}}$ $\times 10^{50} \text{ (ergs)}$
1	12 26 13.7	48 29 46.0	294	11	3	90	439	19.5	0.8	1.0	1.0	20	1.66	1.83
2	12 26 15.3	48 30 7.0	268	13	3	13	405	15.2	0.8	1.6	0.6	18	1.73	2.05

Table 29. Hole Properties of Haro 36

Hole No.	RA (J2000) (h m s)	Dec (J2000) (d m s)	v_{hel} (km s ⁻¹)	v_{exp} (km s ⁻¹)	Hole Type	PA (deg)	d (pc)	Age (Myr)	$\log N_{\text{H I}}$ ($\times 10^{20} \text{ cm}^{-2}$)	R (kpc)	Axial Ratio	H I mass $\times 10^4 M_{\odot}$	$\log E_{\text{Mc}}$ $\times 10^{50} (\text{ergs})$	$\log E_{\text{Ch}}$ $\times 10^{50} (\text{ergs})$
1	12 46 54.1	51 36 26.1	541	18	3	90	1137	30.9	1.2	1.5	1.0	1978	3.91	3.89

Table 30. Hole Properties of IC 10

Hole No.	RA (J2000) (h m s)	Dec (J2000) (d m s)	v_{hel} (km s ⁻¹)	v_{exp} (km s ⁻¹)	Hole Type	PA (deg)	d (pc)	Age (Myr)	$\log N_{\text{HI}}$ ($\times 10^{20} \text{ cm}^{-2}$)	R (kpc)	Axial Ratio	H I mass $\times 10^4 M_{\odot}$	$\log E_{\text{Mc}}$ $\times 10^{50} \text{ (ergs)}$	$\log E_{\text{Ch}}$ $\times 10^{50} \text{ (ergs)}$
1	00 19 52.1	59 18 5.1	-371	13	3	90	81	3.1	1.0	0.9	1.0	0	0.04	1.08
2	00 19 53.2	59 17 30.6	-361	20	2	9	83	2.0	1.1	0.9	0.5	1	0.36	1.69
3	00 20 0.3	59 17 51.5	-355	16	1	15	250	7.6	0.9	0.7	0.7	9	1.56	2.21
4	00 20 6.3	59 19 33.8	-361	16	1	85	129	3.9	1.0	0.6	0.6	1	0.72	1.70
5	00 20 10.7	59 16 59.3	-355	16	1	2	200	6.1	1.0	0.4	0.3	5	1.34	2.09
6	00 20 13.4	59 17 44.3	-350	16	1	151	181	5.5	0.9	0.3	0.7	3	1.08	1.89
7	00 20 15.2	59 16 50.3	356	16	1	10	135	4.1	1.0	0.3	0.7	2	0.80	1.75
8	00 20 16.7	59 19 36.9	-340	16	1	174	225	6.9	1.0	0.4	0.7	7	1.46	2.16
9	00 20 17.3	59 18 39.9	-361	26	2	90	51	1.0	1.0	0.2	1.0	0	-0.21	1.55
10	00 20 22.0	59 18 26.4	-340	16	1	139	237	7.2	1.0	0.2	0.7	10	1.61	2.28
11	00 20 22.2	59 17 29.4	-340	16	1	134	68	2.1	1.3	0.0	0.6	0	0.18	1.43
12	00 20 23.8	59 17 12.9	-340	16	1	12	46	1.4	1.3	0.1	0.8	0	-0.35	1.09
13	00 20 27.5	59 19 57.2	-350	25	2	73	97	1.9	1.0	0.6	0.9	1	0.64	2.06
14	00 20 28.5	59 21 6.9	-335	16	1	177	146	4.5	1.2	0.9	0.8	3	1.08	1.98
15	00 20 28.7	59 19 20.4	-325	16	1	5	127	3.9	1.0	0.5	0.9	1	0.72	1.69
16	00 20 33.8	59 20 9.8	-330	16	1	38	118	3.6	1.0	0.8	0.6	1	0.66	1.67
17	00 20 42.2	59 17 24.8	-340	16	1	46	193	5.9	1.0	0.6	0.6	5	1.28	2.04
18	00 20 44.8	59 19 17.2	-325	25	2	42	57	1.1	1.2	0.9	0.7	0	0.11	1.76
19	00 20 46.7	59 19 53.2	-335	16	1	130	135	4.1	1.1	1.0	0.7	2	0.89	1.82
20	00 20 47.1	59 18 15.7	-335	15	2	112	93	3.0	1.1	0.8	0.4	1	0.38	1.45

Table 31. Hole Properties of IC 1613

Hole No.	RA (J2000) (h m s)	Dec (J2000) (d m s)	v_{hel} (km s ⁻¹)	v_{exp} (km s ⁻¹)	Hole Type	PA (deg)	d (pc)	Age (Myr)	$\log N_{\text{H I}}$ ($\times 10^{20} \text{ cm}^{-2}$)	R (kpc)	Axial Ratio	H I mass $\times 10^4 M_{\odot}$	$\log E_{\text{Mc}}$ $\times 10^{50} \text{ (ergs)}$	$\log E_{\text{Ch}}$ $\times 10^{50} \text{ (ergs)}$
1	01 04 31.8	02 07 24.8	-234	6	1	120	745	60.7	0.5	0.9	0.3	165	1.88	1.38
2	01 04 37.1	02 10 8.3	-239	6	1	140	425	34.6	0.6	0.9	0.5	16	1.20	0.96
3	01 04 48.8	02 12 41.3	-229	6	1	60	634	51.7	0.4	1.2	0.7	105	1.59	1.18
4	01 04 49.2	02 03 29.3	-229	6	1	144	209	17.1	0.6	1.1	0.7	2	0.30	0.40
5	01 04 54.6	02 07 14.3	-244	6	1	132	821	66.9	0.6	0.3	0.6	297	2.20	1.63
6	01 04 53.4	02 03 35.3	-234	6	1	90	143	11.6	0.7	1.1	1.0	1	-0.11	0.17
7	01 04 58.4	02 09 26.3	-229	6	1	144	172	14.0	1.2	0.6	0.8	4	0.64	0.78
8	01 05 3.3	02 11 14.3	-229	6	1	164	295	24.1	0.9	1.1	0.5	11	1.04	0.97
9	01 05 4.4	02 09 17.3	-229	6	1	154	163	13.3	1.1	0.8	0.7	3	0.52	0.69
10	01 05 6.0	02 07 29.3	-229	6	1	132	156	12.7	0.9	0.9	0.7	2	0.26	0.46
11	01 05 9.7	02 09 35.3	-229	6	1	171	191	15.6	0.9	1.1	0.7	4	0.54	0.65

Table 32. Hole Properties of LGS 3

Hole No.	RA (J2000) (h m s)	Dec (J2000) (d m s)	v_{hel} (km s ⁻¹)	v_{exp} (km s ⁻¹)	Hole Type	PA (deg)	d (pc)	Age (Myr)	$\log N_{\text{H I}}$ ($\times 10^{20} \text{ cm}^{-2}$)	R (kpc)	Axial Ratio	H I mass $\times 10^4 M_{\odot}$	$\log E_{\text{Mc}}$ $\times 10^{50} \text{ (ergs)}$	$\log E_{\text{Ch}}$ $\times 10^{50} \text{ (ergs)}$
1	01 03 51.1	21 52 21.5	-289	5	1	35	47	4.6	-0.3	0.5	0.6	0	-2.51	-1.73
2	01 03 51.4	21 52 5.0	-297	5	1	47	40	3.9	-0.3	0.4	0.4	0	-2.80	-1.92
3	01 03 56.7	21 53 6.5	-294	5	1	28	27	2.7	-0.1	0.2	0.6	0	-3.08	-2.06
4	01 03 57.5	21 53 24.5	-290	7	3	90	57	4.0	-0.2	0.3	1.0	0	-1.92	-1.01
5	01 03 58.2	21 52 30.5	-292	5	1	43	32	3.1	-0.2	0.3	0.5	0	-2.96	-2.01
6	01 03 58.8	21 53 17.0	-284	7	3	164	50	3.5	-0.3	0.4	0.8	0	-2.25	-1.27
7	01 03 59.0	21 52 23.0	-281	10	3	90	37	1.8	-0.2	0.4	1.0	0	-2.38	-1.00

Table 33. Hole Properties of M81dwA

Hole No.	RA (J2000) (h m s)	Dec (J2000) (d m s)	v_{hel} (km s ⁻¹)	v_{exp} (km s ⁻¹)	Hole Type	PA (deg)	d (pc)	Age (Myr)	$\log N_{\text{H I}}$ ($\times 10^{20} \text{cm}^{-2}$)	R (kpc)	Axial Ratio	H I mass $\times 10^4 M_{\odot}$	$\log E_{\text{Mc}}$ $\times 10^{50} (\text{ergs})$	$\log E_{\text{Ch}}$ $\times 10^{50} (\text{ergs})$
1	08 23 40.9	71 01 52.4	107	8	3	90	306	18.7	0.3	1.4	1.0	2	0.34	0.52
2	08 23 45.8	71 01 26.9	118	10	2	90	204	10.0	0.2	1.1	1.0	1	-0.12	0.43
3	08 23 53.5	71 02 10.5	113	7	1	78	1177	82.2	0.3	0.6	0.6	217	2.08	1.51
4	08 23 53.8	71 00 58.5	110	8	3	90	244	14.9	0.4	1.3	1.0	1	0.15	0.44
5	08 23 56.9	71 01 4.5	107	9	3	48	294	16.0	0.5	1.1	0.6	3	0.59	0.86
6	08 24 2.7	71 01 2.9	122	10	3	40	253	12.4	0.4	1.3	0.8	2	0.40	0.82
7	08 24 3.3	71 01 28.4	108	8	3	90	204	12.5	0.5	0.8	1.0	1	0.04	0.40
8	08 24 5.2	71 01 31.4	113	10	3	90	183	9.0	0.4	0.8	1.0	1	-0.06	0.52
9	08 24 7.3	71 01 44.9	112	9	3	90	183	10.0	0.4	0.9	1.0	1	-0.16	0.34
10	08 24 10.1	71 02 13.4	112	8	3	52	355	21.7	0.4	1.2	0.8	4	0.64	0.75

Table 34. Hole Properties of Mrk 178

Hole No.	RA (J2000) (h m s)	Dec (J2000) (d m s)	v_{hel} (km s ⁻¹)	v_{exp} (km s ⁻¹)	Hole Type	PA (deg)	d (pc)	Age (Myr)	$\log N_{\text{HI}}$ ($\times 10^{20} \text{ cm}^{-2}$)	R (kpc)	Axial Ratio	H I mass $\times 10^4 M_{\odot}$	$\log E_{\text{Mc}}$ $\times 10^{50} \text{ (ergs)}$	$\log E_{\text{Ch}}$ $\times 10^{50} \text{ (ergs)}$
1	11 33 27.5	49 14 23.0	253	16	2	168	357	10.9	0.9	0.6	0.7	8	1.49	2.03

Table 35. Hole Properties of NGC 1569

Hole No.	RA (J2000) (h m s)	Dec (J2000) (d m s)	v_{hel} (km s ⁻¹)	v_{exp} (km s ⁻¹)	Hole Type	PA (deg)	d (pc)	Age (Myr)	$\log N_{\text{H I}}$ ($\times 10^{20} \text{ cm}^{-2}$)	R (kpc)	Axial Ratio	H I mass $\times 10^4 M_{\odot}$	$\log E_{\text{Mc}}$ $\times 10^{50} \text{ (ergs)}$	$\log E_{\text{Ch}}$ $\times 10^{50} \text{ (ergs)}$
1	04 30 48.3	64 50 58.1	-73	22	1	54	287	6.4	1.5	0.2	0.7	28	2.28	3.06
2	04 30 50.0	64 50 41.5	-73	22	1	125	351	7.8	1.3	0.3	0.7	31	2.32	3.02
3	04 30 50.0	64 51 25.0	-48	26	3	90	257	4.8	1.5	1.1	1.0	20	2.23	3.18
4	04 30 52.5	64 50 32.3	-57	30	2	179	258	4.2	1.4	0.5	0.7	16	2.23	3.27
5	04 31 0.0	64 50 27.3	-58	22	1	45	228	5.1	1.5	1.2	0.7	14	1.98	2.87

Table 36. Hole Properties of NGC 2366

Hole No.	RA (J2000) (h m s)	Dec (J2000) (d m s)	v_{hel} (km s ⁻¹)	v_{exp} (km s ⁻¹)	Hole Type	PA (deg)	d (pc)	Age (Myr)	$\log N_{\text{H I}}$ ($\times 10^{20} \text{ cm}^{-2}$)	R (kpc)	Axial Ratio	H I mass $\times 10^4 M_{\odot}$	$\log E_{\text{Mc}}$ $\times 10^{50} \text{ (ergs)}$	$\log E_{\text{Ch}}$ $\times 10^{50} \text{ (ergs)}$
1	07 28 32.3	69 11 4.0	71	10	2	136	427	20.9	1.3	2.5	0.5	22	1.65	1.76
2	07 28 34.3	69 10 59.5	64	11	1	90	475	21.1	1.3	2.1	1.0	25	1.76	1.88
3	07 28 41.3	69 12 7.0	86	11	1	136	632	28.1	1.3	1.5	0.9	67	2.20	2.19
4	07 28 41.6	69 11 31.0	77	11	3	90	297	13.2	1.4	1.1	1.0	9	1.30	1.63
5	07 28 44.4	69 10 34.1	74	6	2	90	327	26.6	1.4	2.7	1.0	10	1.00	0.88
6	07 28 50.3	69 12 11.6	98	10	2	90	257	12.6	1.4	0.7	1.0	6	1.04	1.39
7	07 28 51.2	69 12 37.1	97	11	1	4	189	8.4	1.4	0.4	0.5	2	0.64	1.21
8	07 28 54.3	69 13 25.1	113	7	2	90	297	20.7	1.5	1.2	1.0	10	1.08	1.11
9	07 28 54.5	69 12 53.6	110	5	3	90	376	36.8	1.4	0.9	1.0	18	1.15	0.83
10	07 28 57.6	69 12 37.1	115	15	2	90	376	12.3	1.5	1.8	1.0	21	1.89	2.32
11	07 28 59.6	69 13 11.6	115	11	1	135	246	10.9	1.5	1.7	0.3	6	1.18	1.58

Table 37. Hole Properties of NGC 3738

Hole No.	RA (J2000) (h m s)	Dec (J2000) (d m s)	v_{hel} (km s ⁻¹)	v_{exp} (km s ⁻¹)	Hole Type	PA (deg)	d (pc)	Age (Myr)	$\log n_{\text{H I}}$ ($\times 10^{20} \text{ cm}^{-2}$)	R (kpc)	Axial Ratio	H I mass $\times 10^4 M_{\odot}$	$\log E_{\text{Mc}}$ $\times 10^{50} \text{ (ergs)}$	$\log E_{\text{Ch}}$ $\times 10^{50} \text{ (ergs)}$
1	11 35 45.7	54 31 11.0	234	18	1	90	399	10.8	1.1	0.7	1.0			
2	11 35 50.4	54 31 17.0	210	18	1	42	378	10.3	1.1	0.3	0.7			
3	11 35 52.5	54 32 6.5	206	18	1	179	340	9.2	1.1	1.3	0.6			

Table 38. Hole Properties of NGC 4214

Hole No.	RA (J2000) (h m s)	Dec (J2000) (d m s)	v_{hel} (km s ⁻¹)	v_{exp} (km s ⁻¹)	Hole Type	PA (deg)	d (pc)	Age (Myr)	$\log N_{\text{H I}}$ ($\times 10^{20} \text{ cm}^{-2}$)	R (kpc)	Axial Ratio	H I mass $\times 10^4 M_{\odot}$	$\log E_{\text{Mc}}$ $\times 10^{50} \text{ (ergs)}$	$\log E_{\text{Ch}}$ $\times 10^{50} \text{ (ergs)}$
1	12 15 22.9	36 21 26.9	272	11	3	90	594	26.4	0.9	3.6	1.0	74	2.28	2.27
2	12 15 25.2	36 18 52.4	259	9	1	90	2334	126.8	0.9	2.8	0.6	4382	4.00	3.20
3	12 15 28.4	36 16 16.4	272	9	1	129	805	43.8	0.8	3.5	0.6	502	2.54	2.26
4	12 15 31.3	36 21 11.9	290	20	2	142	454	11.1	1.1	2.1	0.8	54	2.51	3.03
5	12 15 32.0	36 20 22.4	270	9	1	90	716	38.9	1.0	1.6	1.0	595	2.58	2.33
6	12 15 35.6	36 23 25.5	301	9	1	47	527	28.6	0.8	3.4	0.9	49	1.95	1.87
7	12 15 35.9	36 18 10.5	267	9	1	159	614	33.4	0.9	1.4	0.9	347	2.26	2.10
8	12 15 37.7	36 17 4.5	277	9	1	90	742	40.3	0.9	2.3	1.0	546	2.56	2.29
9	12 15 40.1	36 19 17.8	301	9	1	90	262	14.2	1.3	0.4	1.0	17	1.51	1.72
10	12 15 40.2	36 21 42.0	306	9	1	90	1104	60.0	0.9	1.8	0.6	1208	3.08	2.64
11	12 15 41.7	36 20 10.5	308	16	3	90	541	16.5	1.0	0.7	1.0	80	2.54	2.83
12	12 15 42.6	36 17 58.5	295	9	1	90	393	21.3	1.1	1.6	1.0	36	1.84	1.87
13	12 15 43.5	36 19 30.7	324	18	2	164	383	10.4	1.1	0.9	0.6	38	2.30	2.81
14	12 15 46.0	36 22 1.4	321	9	1	111	1014	55.1	0.8	2.4	0.4	703	2.80	2.40
15	12 15 47.3	36 20 28.4	329	9	1	109	1054	57.3	0.9	1.7	0.6	995	2.98	2.55
16	12 15 47.6	36 16 37.3	306	9	1	177	263	14.3	1.0	3.2	0.7	9	1.23	1.46
17	12 15 50.5	36 18 34.4	311	20	2	22	679	16.6	1.0	2.4	0.5	502	2.96	3.30
18	12 15 53.5	36 21 50.9	324	12	2	106	856	34.9	0.8	3.3	0.6	475	2.72	2.61
19	12 15 54.6	36 19 14.9	332	9	1	90	611	33.2	0.9	3.0	1.0	352	2.26	2.10
20	12 15 55.1	36 16 47.9	311	9	1	90	873	47.4	0.8	4.1	1.0	530	2.60	2.28
21	12 15 56.0	36 20 26.9	327	9	1	90	698	37.9	0.8	3.3	1.0	381	2.36	2.14

Table 39. Hole Properties of SagDIG

Hole No.	RA (J2000) (h m s)	Dec (J2000) (d m s)	v_{hel} (km s ⁻¹)	v_{exp} (km s ⁻¹)	Hole Type	PA (deg)	d (pc)	Age (Myr)	$\log N_{\text{HI}}$ ($\times 10^{20} \text{ cm}^{-2}$)	R (kpc)	Axial Ratio	H I mass $\times 10^4 M_{\odot}$	$\log E_{\text{Mc}}$ $\times 10^{50} \text{ (ergs)}$	$\log E_{\text{Ch}}$ $\times 10^{50} \text{ (ergs)}$
1	19 29 56.1	-17 41 41.9	-79	9	1	125	666	36.2	0.4	0.6	0.8	8	1.04	0.99

Table 40. Hole Properties of UGC 8508

Hole No.	RA (J2000) (h m s)	Dec (J2000) (d m s)	v_{hel} (km s ⁻¹)	v_{exp} (km s ⁻¹)	Hole Type	PA (deg)	d (pc)	Age (Myr)	$\log N_{\text{H I}}$ ($\times 10^{20} \text{ cm}^{-2}$)	R (kpc)	Axial Ratio	H I mass $\times 10^4 M_{\odot}$	$\log E_{\text{Mc}}$ $\times 10^{50} \text{ (ergs)}$	$\log E_{\text{Ch}}$ $\times 10^{50} \text{ (ergs)}$
1	13 30 37.2	54 55 19.4	45	8	3	162	117	7.2	0.9	1.1	0.6	1	0.04	0.58
2	13 30 38.8	54 54 46.4	49	8	3	90	121	7.4	0.9	0.7	1.0	1	0.04	0.59
3	13 30 46.3	54 54 30.0	71	8	1	173	262	16.0	1.3	0.2	0.5	19	1.49	1.61

Table 41. Hole Properties of WLM

Hole No.	RA (J2000) (h m s)	Dec (J2000) (d m s)	v_{hel} (km s ⁻¹)	v_{exp} (km s ⁻¹)	Hole Type	PA (deg)	d (pc)	Age (Myr)	$\log N_{\text{HI}}$ ($\times 10^{20} \text{ cm}^{-2}$)	R (kpc)	Axial Ratio	H I mass $\times 10^4 M_{\odot}$	$\log E_{\text{Mc}}$ $\times 10^{50} \text{ (ergs)}$	$\log E_{\text{Ch}}$ $\times 10^{50} \text{ (ergs)}$
1	00 01 56.1	-15 28 57.0	-108	10	1	94	105	5.1	1.3	0.8	0.7	1	0.46	1.17
2	00 01 58.5	-15 27 41.8	-119	10	1	139	189	9.2	1.4	0.1	0.9	9	1.30	1.72
3	00 01 58.9	-15 28 49.5	-113	10	1	90	102	5.0	1.4	0.3	1.0	2	0.49	1.21
4	00 02 3.7	-15 31 12.0	-98	10	1	90	268	13.1	1.1	1.3	1.0	34	1.43	1.72

REFERENCES

- Angeretti, L., Tosi, M., Greggio, L., Sabbi, E., Aloisi, A., & Leitherer, C. 2005 AJ, 129, 2203
- Bagetakos, I., Brinks, E., Walter, F., de Blok, W. J. G., Usero, A., Leroy, A. K., Rich, J. W., & Kennicutt, R. C. 2011 AJ, 141, 23
- Brinks, E., & Bajaja, E. 1986, A&A, 169, 14
- Cannon, J. M., Most, H. P., Skillman, E. D., Weisz, D. R., Cook, D., Dolphin, A. E., Kennicutt, R. C., Lee, J., Seth, A., Walter, F., & Warren, S. R. 2011, ApJ, 735, 36
- Cash, W., Charles, P., Bowyer, S., Walter, F., Garmire, G., & Riegler, G. 1980 ApJ, 238, L71
- Castor, J., McCray, R., & Weaver, R. 1975 ApJL, 200, L07
- Chakraborti, S., & Ray, A. 2011, ApJ, 728, 24
- Chevalier, R. A. 1974, ApJ, 188, 501
- Chu, Y.-H. 2008, in IAU Symp. 250, *Massive Stars as Cosmic Engines*, ed. F. Bresolin, P. A. Crowther, & J. Puls (Cambridge: Cambridge Univ. Press), 341
- Cox, D. P., & Smith, B. W. 1974, ApJ, 189, 105
- Cowie, L. L., Songaila, A., Hu, E. M., & Cohen, J. G. 1996 AJ, 112, 839
- Daigle, A., Joncas, G., Parizeau, M., & Miville-Deschênes, M. 2003, PASP, 115, 662
- Deharveng, L., Zavagno, A., Schuller, F., Caplan, J., Pomarès, M., & De Breuck, C. 2009, A&A, 496, 177
- Dellenbusch, K. E., Gallagher, III, J. S., Knezek, P. M., & Noble, A. G. 2008 AJ, 135, 326
- de Vaucouleurs, G., de Vaucouleurs, A., Corwin, Jr., H. G., Buta, R. J., Paturel, G., & Fouque, P. 1991, S&T, 82, 621
- Dib, S., & Burkert, A. 2005, ApJ, 630, 238
- Dohm-Palmer, R. C., Skillman, E. D., Saha, A., Tolstoy, E., Mateo, M., Gallagher, J., Hoessel, J., Chiosi, C., & Dufour, R. J. 1997 AJ114, 2527
- Dumas, G., Schinnerer, E., Tabatabaei, F. S., Beck, R., Velusamy, T., & Murphy, E. 2011, AJ, 141, 41
- Dyson, J. E. 1977, A&A, 59, 161
- Efremov, Y. N., Elmegreen, B. G., & Hodge, P. W. 1998, ApJ, 501, L163
- Ehlerová, S. & Palouš, J. 2005, A&A, 437, 101
- Ehlerová, S. & Palouš, J. 2013, A&A, 550, A23
- Ehlerová, S. & Palouš, J. 2016, A&A, 587, A5
- Frick, P., Beck, R., Berkhuijsen, E. M., & Patrickeyev, I. 2001, MNRAS, 327, 1145
- Gil de Paz, A., et al. 2007, ApJS, 173, 185
- Gooch, R.E., 1996, *Astronomical Data Analysis Software and Systems V*, ASP Conf. Series vol. 101, eds. G.H. Jacoby & J. Barnes, ASP, San Francisco, p80-83, ISSN 1080-7926
- Heiles, C. 1976, ApJL, 208, L137
- Heiles, C. 1979, ApJ, 229, 533
- Heiles, C. 1984, ApJS, 55, 585
- Herrmann, K. A., Hunter, D. A., & Elmegreen, B. G. 2013, AJ, 146, 5
- Hindman, J. V. 1967, AuJPh, 20, 147
- Hoffman, G. L., Salpeter, E. E. & Carle, N. J. 2001, AJ, 122, 2428
- Hu, E. M., 1981, ApJ, 248, 119
- Hughes, A., Wong, T., Staveley-Smith, L., Filipovic, M., Maddison, S., Fukui, Y., & Mizuno, N. 2006, MNRAS, 370, 363
- Hunter, D. A. 1982, ApJ, 260, 81
- Hunter, D. A., & Elmegreen, B. G. 2004, ApJ, 128, 2170
- Hunter, D. A. & Elmegreen, B. G. 2006, ApJS, 162, 49
- Hunter, D. A., Elmegreen, B. G., & Baker, A. L. 1998, ApJ, 493, 595
- Hunter, D. A., Elmegreen, B. G., & Ludka, B. C. 2010, AJ, 139, 447
- Hunter, D. A., Ficut-Vicas, D., Ashley, T., Brinks, E., Cigan, P., Elmegreen, B. G., Heesen, V., Herrmann, K. A., Johnson, M., Oh, S.-H., Rupen, M. P., Schrubba, A., Simpson, C. E., Walter, F., Westpfahl, D. J., Young, L. M., & Zhang, H.-X. 2012, AJ, 144, 134
- Hunter, D. A., & Plummer, J. D. 1996, ApJ, 462, 732
- Kaisin, S. S., & Karachentsev, I. D. 2008, A&A, 479, 603
- Karachentsev, I. D., Karachentseva, V. E., Huchtmeier, W. K., & Makarov, D. I. 2004, AJ, 127, 2031
- Kauffmann, G., Charlot, S., & White, S. D. 1996, MNRAS, 283, L117
- Kauffmann, G., White, S. D., & Guiderdoni, B. 1993, MNRAS, 264, 201
- Kennicutt, R. C., Jr. 1989, ApJ, 344, 685
- Kennicutt, Jr., R. C., Bresolin, F., Bomans, D. J., Bothun, G. D., & Thompson, I. B. 1995, AJ, 109, 594
- Kennicutt, R. C., & Evans, N. J. 2012, ARA&A, 50, 531
- Kim, S., Dopita, M. A., Staveley-Smith, L., & Bessell, M. S. 1999, AJ, 118, 2797
- Klein, U. 2012, in *Dwarf Galaxies: Keys to Galaxy Formation and Evolution*, ed. P. Papaderos, S. Recchi, & G. Hensler (Berlin: Springer), 23
- Larsen, S. S., Origlia, L., Brodie, J., & Gallagher, J. S. 2008, MNRAS, 383, 263
- Loeb, A., & Perna, R. 1998, ApJ, 503, L35
- Lozinskaya, T. A., Moiseev, A. V., & Podorvanyuk, N. Y. 2003, Astronomy Letters, 29, 77
- Martin, C. L. 1998, ApJ, 506, 222
- Mashchenko, S., & St-Louis, N. 2002, in ASP Conf. Ser. 260, *Interacting Winds from Massive Stars*, ed. A. F. J. Moffat & N. St-Louis (San Francisco, CA: ASP), 65
- Mateo, M. L. 1998, ARA&A, 36, 435

- McCray, R., & Kafatos, M. 1987, *ApJ*, 317, 190
- McKee, C. F., & Ostriker, J. P. 1977, *ApJ*, 218, 148
- Murray, S. D. & Lin, D. N. C. 2004, *ApJ*, 615, 586
- Oey, M. S., 2007, *Towards Resolving the Evolution of Multi-supernova Superbubbles*, Series: IAU Symposium, DOI 10.1017/S1743921307001305, eds. Elmegreen, B. G., & Palous, J., 237, 106
- Oey, M. S., & Clarke, C. J. 1997, *MNRAS*, 289, 570
- Ott, J., Walter, F., Brinks, E., Van Dyk, S. D., Dirsch, B., & Klein, U. 2001, *AJ*, 122, 3070
- Park, G., Koo, B.-C., Kang, J.-h., et al. 2016, *ApJL*, 827, L27
- Perna, R. & Raymond, J. 2000, *ApJ*, 539, 706
- Pidopryhora, Y., Lockman, F. J., & Shields, J. C. 2007, *ApJ*, 656, 928
- Puche, D., Westpfahl, D., Brinks, E., & Roy, J.-R. 1992, *AJ*, 103, 1841
- Rand, R.J. & Stone, J. M. 1996, *AJ*, 111, 190
- Relaño, M., Beckman, J., Daigle, O. & Carignan, C. 2007, *A&A*, 467, 1117
- Sallmen, S. M., Korpela, E. J., Bellehumeur, B., et al. 2015, *AJ*, 149, 189
- Santillán, A., Franco, J., Martos, M. & Kim, J. 1999, *ApJ*, 515, 657
- Silitch, S., Lozinskaya, T., Moiseev, A., et al. 2006, *A&A*, 448, 123
- Silk, J. 1997, *ApJ*, 481, 703
- Simon, J. D. 2019, *Annual Review of Astronomy & Astrophysics*, 57, 375
- Simpson, C. E., Hunter, D. A., & Knezek, P. M. 2005a, *AJ*, 129, 160
- Simpson, C. E., Hunter, D. A. & Nordgren, T. E. 2005b, *AJ*, 130, 1049
- Simpson, C. E., Hunter, D. A., Nordgren, T. E., Brinks, E., Elmegreen, B. G., Ashley, T., Lynds, R., McIntyre, V. J., O’Neil, E. J., Östlin, G., Westpfahl, D. J., & Wilcots, E. M. 2011, *AJ*, 142, 82
- Skillman, E. D., 1996, *Neutral Hydrogen in Dwarf Galaxies*, Series: Astronomical Society of the Pacific Conference, ed., Skillman E. D., 106, 208
- Stil, J. M. & Israel, F. P. 2002, *A&A*, 389, 29
- Suad, L. A., Caiafa, C. F., Arnal, E. M., & Cichowolski, S. 2014, *A&A*, 564, A116
- Suad, L. A., Cichowolski, S., Noriega-Crespo, A., et al. 2016, *A&A*, 585, A154
- Tabatabaei, F. S., Beck, R., Krause, M., Berkhuijsen, E. M., Gehrz, R., Gordon, K. D., Hinz, J. L., Humphreys, R., McQuinn, K., Polonski, E., Rieke, G. H., & Woodward, C. E. 2007, *A&A*, 466, 509
- Tenorio-Tagle, G. 1981, *A&A*, 94, 338
- Tenorio-Tagle, G., & Bodenheimer, P. 1988, *A&A*, 26, 145
- Thilker, D. A., Braun, R., & Walterbos, R. A. M. 1998, *A&A*, 332, 429
- Thilker, D. A., et al. 2007, *ApJS*, 173, 538
- Thilker, D. A., et al. 2008, in *ASP Conf. Ser.* 396, *Formation and Evolution of Galaxy Disks*, ed. J. G. Funes, S.J., and E. M. Corsini. (San Francisco, CA: ASP), 223
- Thomas, D., Maraston, C., Bender, R., & Mendes de Oliveira, C. 2005, *ApJ*, 621, 673
- Tolstoy, E., Hill, V., & Tosi, M. 2009, *Annual Review of Astronomy & Astrophysics*, 47, 371
- van den Bergh, S. 2000, in *Cambridge Astroph. Ser. Vol. 35, The Galaxies of the Local Group*, Cambridge University Press, Cambridge, UK
- van Zee, L. 2000, *ApJL*, 543, L31
- Vorobyov, E. I., & Basu, S. 2005, *A&A*, 431, 451
- Walter, F., & Brinks, E. 1999, *AJ*, 118, 273
- Walter, F., & Brinks, E. 2001, *AJ*, 121, 3026
- Walter, F., Weiss, A., Martin, C., & Scoville, N. 2002, *AJ*, 123, 225
- Warren, S. R., Weisz, D. R., Skillman, E. D., Cannon, J. M., Dalcanton, J. J., Dolphin, A. E., Kennicutt, R. C., Jr., Koribalski, B., Ott, J., Stilp, A. M., Van Dyk, S. D., Walter, F., & West, A. A. 2011, *ApJ*, 738, 10
- weaver, R., & Williams, D. R. W. 1973, *A&AS*, 8, 1
- Weaver, R., McCray, R., Castor, J., Shapiro, P., & Moore, R. 1977, *ApJ*, 218, 377
- Weisz, D. R., Skillman, E. D., Cannon, J. M., Walter, F., Brinks, E., Ott, J., & Dolphin, A. E. 2009a, *ApJL*, 691, L59
- Weisz, D. R., Skillman, E. D., Cannon, J. M., Dolphin, A. E., Kennicutt, R. C., Lee, J., & Walter, F. 2009b, *ApJ*, 704, 1538
- Westerlund, B. E., & Mathewson, D. S. 1966, *MNRAS*, 131, 371
- Wilcots, E. M. & Miller, B. W. 1998, *AJ*, 116, 2363